INSTYTUT FIZYKI JĄDROWEJ
INSTITUTE OF NUCLEAR PHYSICS
ИНСТИТУТ ЯДЕРНОЙ ФИЗИКИ

KRAKÓW

PL9000...

RAPORT No 1371/PL

TWO LECTURES ON TRACK STRUCTURE

WALIGÓRSKI MICHAŁ

KRAKÓW 1987

TWO LECTURES ON TRACK STRUCTURE

Michael P. R. Waligórski

Institute of Nuclear Physics

Radzikowskiego 152, 31-342 Kraków, Poland

WYDANO NAKŁADEM
INSTYTUTU FIZYKI JĄDROWEJ W KRAKOWIE
UL. RADZIKOWSKIEGO 152
NA PRAWACH RĘKOPISU

Kopię kserograficzną, druk i oprawę wykonano w IFJ Kraków

Wydanie I *Zam. 194/87* *Nakład 85 egz.*

ABSTRACT

In a series of two lectures the principles of track structure theory, developed by Katz and collaborators, are reviewed. The text is intended to serve as an introduction to the theory. Applications of the model to c-hit physical detectors and to biological systems are reviewed. The model relates the signal of a detector after doses of X and gamma radiations to its signal after heavy charged particle irradiations, and is applicable to a variety of physical dosimeters : alanine, thermoluminescence and the Fricke dosimeters, to the inactivation of enzymes and viruses, and to biological systems: description of survival and neoplastic transformations in mammalian cells. Application of the model to heavy-ion cancer radiotherapy and to radiation protection are discussed as well as the controversies around the track structure approach. The model suggests new insights to fundamental research in detector theory and in radiobiology and in their applications in radiotherapy and radiation protection.

DWA WYKŁADY O TEORII STRUKTURY ŚLADU

Streszczenie

W formie dwóch wykładów przedstawiono podstawy teorii struktury śladu, modelu opracowanego przez Katza i współpracowników. Praca niniejsza ma służyć jako wprowadzenie w podstawy teorii. Omówiono zastosowanie tego modelu do c-hitowych detektorów fizycznych oraz do układów biologicznych. Model wiąże sygnał detektora po naświetleniu go dawkami promieni X lub gamma z sygnałem tego detektora po napromienieniu go ciężkimi cząstkami naładowanymi. Model stosuje się do wielu detektorów fizycznych : dawkomierza alaninowego, dawkomierzy termoluminescencyjnych, dozymetru Frickego, do inaktywacji enzymów i wirusów, oraz , w układach biologicznych, do opisu przeżywalności i indukcji transformacji nowotworowych w kulturach komórek ssaków. Omówiono zastosowanie modelu w radioterapii nowotworowej ciężkimi jonami, oraz w zagadnieniu ochrony przed promieniowaniem, przedstawiono również kontrowersje wokół modelu struktury śladu. Model ten sugeruje nowe podejście do badań podstawowych w dziedzinie teorii detekcji promieniowania jądrowego i radiobiologii, oraz ich zastosowań w dozymetrii, radioterapii nowotworowej i ochronie przed promieniowaniem.

ДВА ДОКЛАДА ПО ТЕОРИИ СТРУКТУРЫ ТРЕКА

Содержание

Принципы теории структуры трека, модели разработанной Катзом и сотрудниками, представлены в форме двух докладов. Предлагаемая работа служит введением к принципам теории. В ней представлено использование модели в физически "с-ударны" детектора а также в биодогически система. Модель связывает сигнал детектора (после его облучения дозами X- или гамма-лучей) с сигналом этого же детектора соответствующим дозе заряженных частиц. Модель используется во многих физических детекторах: аланиновом, ТЛ- и Фрике- дозиметре; для инактивации энзимов и вирусов, а также в биодогических системах : для описания выживания и индукции раковых трансформации в культурах тканей млекопитающих. Представлено также использование модели в раковой радиотерапии тяжелыми ионами, в радиационной защите, а также разногласия связанные с моделю структуры трека. Модель предлагает новый подход к основным исследованиям в теори детекции ядерного излучения и радиобиологии, а также их применение в дозиметрии, раковой радиотерапии и радиационной защите.

ION TRACKS: I. STRUCTURE AND BIOLOGICAL SIGNIFICANCE

Introduction

The seminal paper of Butts and Katz was first published in Radiation Research (1) exactly 20 years ago. Though the track structure theory of RBE, due to the work of Katz and collaborators, has since then greatly expanded in depth and scope (2,3), the principal assumptions of the model outlined in that first paper remain unchanged. The notion that the response of a detector to a beam of heavy charged particles can be described by the single-particle inactivation cross-section, defined as the integral of the radial distribution of inactivation probability, is as valid as ever. The radial distribution of inactivation probability is still calculated as a convolution of the function representing the response of the detector to a "test" radiation (typically, ^{60}Co gamma-rays), and of the function representing the radial distribution of average dose around the path of a heavy ion. The main conclusions of the paper of Butts and Katz were that RBE for 1-hit detectors, such as dry enzymes and viruses, cannot be represented as a single-valued function of LET, and that the theory accounted for experimentally measured values of inactivation cross-sections exceeding geometrical cross-sections of enzyme and virus molecules. The calculations also showed a decline of cross-sections at the stopping end of the particle tracks, i. e. "thindown". These conclusions are only now gaining wider acceptance, having been recently supported by results of radiobiological experiments. In its cellular version (4), the model of Katz has been very successful in describing RBE dependences of the survival of mammalian cells after heavy ion bombardment.

Recently, the formula describing the radial distribution of dose around the particle's path has been somewhat improved (5), leading to a better model description of the response of dry enzymes and viruses (6), the Fricke dosimeter (7) and of alanine (8) to heavy charged particles. Also, the cellular model has been applied to neoplastic transformations in a mammalian cell culture exposed to beams of energetic heavy ions (9) and the implications of these results for radiation protection studied (10), but these subjects will be discussed in the second lecture.

In this lecture I would like to briefly review in a manner as simple as possible the principles of track structure theory, discuss the more recent developments of the model as applied to "1-hit physical detectors" and show some implications of this theory to radiobiology and radiation protection.

Principles of track structure theory

Since particle tracks are best visualized in nuclear emulsion, let us look at some tracks in "grain count", intermediate, and "track width" regimes shown in Fig. 1. Stopping-end parts of some heavy ion tracks in nuclear emulsion are shown in Fig.2. Nuclear emulsion consists of uniform grains of silver halide which could represent radiosensitive targets distributed in a gelatine matrix.

We note that the probability of activating grains along the path of leftmost (lightest) ion is less than one, that of the intermediate track is about one (every grain along the particle's path is activated), while the "hairy rope" appearance of the third track, due to effects of delta-rays accompanying the passage of the heaviest ion, indicates that the probability of grain activation is high even at some distance from the particle's path.

The interesting feature of Fig. 2 is that nowhere is the increase of ionization in the Bragg peak apparent in the appearance of these tracks.

Track structure theory offers a unified description of tracks shown in both figures. Let us, for the sake of our discussion, initially assume that Fig. 1 represents tracks of the same heavy ion in three detectors of different radiosensitivity. Then, Fig. 3 illustrates the principle of the track theory calculation. Panel 1, the upper-right one in Fig. 3, represents the activation probability after uniform irradiation of the detector with test radiation (X-or gamma-rays), i.e. the signal v. dose characteristics normalized to saturation signal. The most radiosensitive detector saturates at the lowest X-ray dose (curve II), while the least sensitive one (curve III) will saturate at higher doses. All curves of activation probability are here represented by the 1-hit formula $P_w(D_w) = 1 - \exp(-D_w/D_0)$, where D_w is the dose of test radiation and D_0 is the characteristic value of saturation dose. The lower-right panel 2 represents the radial distribution of average dose (horizontal axis) v. radial distance (downward axis) for three different ions (H, C and Ne) of the same stopping power (LET). Using this radial distribution of dose, $D_w(r)$, as a transfer function, one is able to calculate the radial distribution of activation probability (shown in panel 3), $P_w(r) = 1 - \exp(-D_w(r)/D_0)$, which corresponds to the density of activated grains around the path of the heavy ion. The appearance of the track of that heavy ion in the least sensitive detector may resemble the "grain count" regime shown in Fig. 1, while passage of the ion through a very sensitive detector would lead to tracks of "track width" appearance.

Actually, in Fig. 1 tracks of three different ions (H, N and Ca) are shown in the same emulsion (Ilford G.5). This would correspond to three different radial distributions of dose (not shown in Fig. 3), that of the Ca ion being displaced towards higher doses (to

the right, in panel 2 of Fig.3) and that for the H ion being the lowest. Now curve I in panel 1 of Fig. 3 could represent the response of the Ilford emulsion, and the resulting radial distributions of activation probability, similar to those shown in panel 3 of the same figure, could explain qualitatively the appearance of particle tracks of Fig. 1.

Two other qualitative statements follow from Fig. 3. Firstly, since above saturation increasing the dose does not lead to any further increase in the response of the detector, regions around the ion's path where the radial dose exceeds, say, the value of D_0, do not contribute to the detector's response to ion doses. It is the relative position of the maximum value of radial dose and the characteristic radiosensitivity of the detector that determines the detector's response to heavy ion doses (or, in other words, the amount of dose "wasted" on saturation "overkill"). If a track of a particle is seen in the grain count regime, no dose is wasted and detection efficiency is high; track width appearance indicates low detection efficiency and high wastage of ion dose. Ion dose alone is not a good parameter for describing detector response.

The second statement follows from the fact that the radial distributions of dose (panel 2 in Fig. 3) calculated for three ions (H, C and Ne) of the same stopping power, are different. The resulting differences in the radial distributions of activation probability are most apparent for the most sensitive detector (II) in the case of the slowest ion, H. Here, the ion velocity-dependent maximum range of the delta-rays begins to limit the width of the particle's track. This is the qualitative explanation of the thindown of particle tracks seen in Fig. 2. The conclusion is that detector efficiency (or RBE) cannot be univocally described by LET alone; knowledge of the ion's charge, velocity and fluence is mandatory.

More generally, track theory states that no simple product of parameters describing the radiation (such as fluence, LET, charge, velocity, or any combination of these) and of parameters describing the detector (such as "hittedness" c or characteristic radiosensitivity D_0) can correctly describe the response (RBE) of the detector to heavy charged particles. Hence, no multiplicative factors, such as the Quality Factor (QF), can properly account for track effects in radiation detectors, including biological systems.

The single-particle activation cross-section through which track theory describes the detector response to charged particle irradiation is a complicated function involving all these parameters in a complex, but mathematically well-defined, manner. It is calculated by volume integration of the radial distribution of activation probability, $\sigma = 2\pi\int r\, P_d(r)\, dr$, over the whole range of radial distances, r.

Response of detectors to test radiation

Track structure calculations outlined above require the assumption that the response of the detector to the dose from delta-rays surrounding the ion's path is the same as that to the dose from the test radiation uniformly distributed throughout the detector volume. Like in target theories well known to radiobiologists, the response of a detector is assumed to arise from hits (e.g. a passage of one or more electrons) to the detector's sensitive targets (e.g. grains of nuclear emulsion). The statistics of target inactivation determines the shape of the response of the detector to doses of test radiation. Two functional forms may be used to represent this response, namely the multi-target and the multi-hit models, shown in Fig. 4. The response of a detector to test radiation dose is then represented by two parameters: number of hits, c (or targets, m) and the value of characteristic saturation dose D_0 at which all targets receive on the average a single hit. For c = m = 1 both forms reduce to the 1-hit formula used to represent the detector response in panel 1 of Fig. 3. Several physical detectors appear to be 1-hit systems, such as the alanine dosimeter (8,11), the response of which to ^{60}Co doses is shown in Fig. 5. The well-known supralinearity in the response of thermoluminescent dosimeters, such as TLD-700, can be interpreted as a superposition of 1-hit and 2-hit traps (12), as shown in Fig. 6.

The response of most cellular systems to doses of ^{60}Co gamma-rays or orthovoltage X-rays can be fitted with the m-target form, where m ranges from c. 2 to c. 3.5 (4). We shall discuss this further in the next lecture.

Though the energy spectrum of delta-ray electrons around the ion's path may be quite different from the spectrum of secondary electrons following gamma-ray irradiation, there is some physical justification for using ^{60}Co gamma rays as the test radiation in track theory calculations. Namely, the shape of the electron slowing-down spectrum over the energy region where electron ionization cross-sections are effective (1-10^{3}eV) is remarkably independent of the initial photoelectron energy, so long as this initial energy is well above, say, 10^{4}eV (13).

Radial distribution of dose

The original expression describing the radial distribution of dose around the path of the heavy ion (1) has been derived on the basis of the Rutherford formula for delta-ray production, assuming normal ejection of delta-rays, a linear energy-range relationship for electrons and an ion velocity-dependent kinematical constraint

limiting the maximum range of delta-rays, i.e. the range of the radial distribution of dose. A well-known formula describing the velocity-dependent "effective charge", Z^*, of an ion of "rest charge" Z, was used[1]. Average dose in concentric cylinders around the ion's path was calculated.

Since then a number of measurements and calculations of radial dose distributions have been made (for references, see (5)). The present formula incorporates the recent results of Monte Carlo calculations of radial distribution of energy for protons of different energy in liquid water (Fig. 7). A relatively simple mathematical formula, featuring a "hump" in the region 1-10 nm, where a power-law energy-range expression is used for electron ranges (14), has been fitted to the calculated distributions of Fig. 7. This formula on integration yields the correct value of proton stopping power over a wide range of proton velocities. The newly developed formula incorporates β-dependent terms in the "hump" and in the maximum range of the distribution (β is the speed of the ion in units of velocity of light), and is the same for all track theory calculations.

The original formula (1) for calculating the effective charge of the ion is still applied to calculate the radial distribution of dose for ions other than protons.

The new formula compares quite favourably with available experimental data, as seen in Fig. 8 where the measured radial distributions of dose are multiplied by the square of the radial distance and by the "effective charge scaling factor" β^2/Z^{*2}. The formula begins to deviate from experimental values at ion energies below 0.5 MeV/amu, indicating the limits of validity of the effective charge formula. One should remember that in the measurements, usually performed in tissue-equivalent gas, a constant value of W, the energy required to form a single electron-ion pair, is assumed. Since W in fact increases somewhat with decreasing energy of the ionizing electron, and since the mean delta-ray energy is known to decrease with decreasing radial distance, the experimental data points of Fig. 8 in the region of the "hump" should in fact be corrected upwards.

Once the "point-target" formula describing the average radial distribution of delta-ray dose in concentric cylinders around the path of a heavy ion is established, one is able to calculate the average dose, $E(t)$, inside a "sensitive site" of radius a_0 whose centre lies at a radial distance t, as shown in Fig. 9. The value of a_0 best fitting all the heavy ion response data for a given detector is the third parameter characterizing this detector.

Once the three parameters of a c-hit detector are established (c and D_0 measured from the response to the test radiation, a_0

---

[1] the formula is given in Fig. 19, eq. (11).

evaluated from the heavy-ion response), one is able to calculate the response of this detector to any radiaton field, via the single-particle activation cross-section, σ.

The "universal" radial distribution of dose and the "kappa" parameter

If the radial distributions of dose of fig. 9 are plotted in "normalized coordinates", i. e. $E(t)a_0^2\beta^2/Z^{*2}$ v. t/a_0, then all these distributions converge into a "universal" distribution which can be shown phenomenologically (2) to be almost independent of the value of a_0 and the ion's effective charge and velocity in the region $t/a_0 < 1$. In most cases, as may be seen in Fig. 10 and Fig. 11, the value of $E(t)a_0^2\beta^2/Z^{*2}$ in this region is about 2×10^{-7}erg/cm. The differences in the regions $t/a_0 > 1$ are due to different β-dependent maximum delta-ray ranges (in units of a_0). Remembering from Fig. 3 that detector saturation effects begin when the value of the radial distribution of dose exceeds D_0, the characteristic radiosensitivity of the detector, we may introduce Katz's "kappa" parameter: $\kappa = D_0a_0^2/(2 \times 10^{-7}\text{erg/cm})$ and analyze the product $Z^{*2}/(\kappa\beta^2)$. The factor Z^{*2}/β^2 describes the properties of the heavy ion, while κ, incorporating D_0 and a_0, describes the properties of the detector. If the value of this parameter is less than 1 (say, below 0.1), there is no detector saturation (grain-count tracks in Fig. 1); if $Z^{*2}/\kappa\beta^2 >> 1$ (say, 10 or more), detector saturation causes the track-width appearance of particle tracks, with possible thindown effects, as seen in Fig. 2. Transition between these two regimes takes place at about $Z^{*2}/\kappa\beta^2 = 4$.

Thus, the kappa parameter offers us a distinction between "high-LET" ($Z^{*2}/\kappa\beta^2>10$) and "low-LET" ($Z^{*2}/\kappa\beta^2<0.1$) radiations <u>with respect to detector properties</u> (as defined by D_0 and a_0), and a "separation" of radiation (Z^{*2}/β^2) and detector (κ) parameters in the specification of the detector response to doses of heavy charged particles. However, in principle, the parameter Z^{*2}/β^2 is no better than LET in describing the detector response to charged particle irradiation, since this response (or RBE) is not a univocal function of Z^{*2}/β^2 either, especially in the region where detector saturation sets in.

Cross-section, relative efficiency and RBE

If the average probability of "non-activation", or "survival" (e.g., the percent of remaining activity for an enzyme) of targets in a 1-hit detector is plotted as a function of dose of test

radiation, D_κ or ion dose, D_i (number of particles per square cm F times LET), one arrives at a set of exponential curves of the type $S(D_\kappa) = \exp(-D_\kappa/D_0)$, or $S(D_i) = \exp(-\sigma F)$. For any given detector, the value of cross-section σ changes with the type or energy of the heavy ion bombardment and can be measured experimentally. A comparison can then be made between values of cross-sections measured experimentally and those calculated from track theory. For dry enzymes and viruses there is excellent agreement between experiment and theoretical calculations made using the present form of the radial distribution of dose (6). An example of such a comparison is shown in Fig. 12, where theoretical calculations were made for ions of different Z at small energy intervals. As demonstrated in the first paper of Butts and Katz (1), there is a "splitting" of cross-sections with LET and a dramatic decrease in the calculated cross-section at the highest values of LET (or Z^{*2}/β^2), i.e at the stopping ends of the particle tracks. This is the thindown of particle tracks, seen in Fig. 2.

For 1-hit detectors there is a simple relationship between RBE at 37% "survival" and the cross-section, namely RBE = σD_0/LET. In the linear part of the dose-response of such a detector, the effectiveness relative to ^{60}Co gamma-rays is simply equal to its RBE (the former is the ratio of signals at the same ion and gamma doses, the latter the ratio of gamma-to-ion doses at the same level of signal).

From an important theoretical constraint proposed by Katz for biological systems, it follows that the RBE (or relative efficiency) for 1-hit detectors cannot exceed 1 (15)[1].

That this rule holds for Fig. 12 is seen by observing that nowhere does the slope of the cross-section curves exceed 1 on this doubly-logarithmic plot (i.e. σ is a linear or sublinear function of LET).

This is not so for the supralinear TLD-700 detector of Fig. 6. A calculation performed for the more supralinear peak 6 in this TLD, the results of which are shown in the lower part of Fig. 13, predicts relative efficiencies greater than 1 in regions close to the residual ranges of heavy ions. This prediction has recently been confirmed experimentally (16).

Detectors showing supralinearity in their test radiation dose response may have the capability of mimicking the response of biological systems to high LET radiations, where RBE can exceed 1. (We shall see later that the maximum value of RBE occurs at $Z^{*2}/\kappa\beta^2$ of about 2). Linear (1-hit) detectors do not have this capability.

---

[1] "The probability of cell killing relative to absorbed dose, after gamma irradiation must be supralinear if an RBE greater than 1 is to be observed for any high LET radiation"

The regular thindown of particle tracks in Fig. 2 indicates that the nuclear emulsion used for imaging these tracks must have had 1-hit properties. If it were a supralinear detector (2-hit, 3-hit, etc.), a region of enhanced track width close to the end of the ion's range would have been visible. The rapidly decreasing effectiveness of the 1-hit emulsion prevents us from seeing the Bragg peak at the particle's residual range.

Simulation of particle tracks

Using a computer randomization technique developed by Furtak and Katz (17) and a calculation based on track theory, tracks of heavy ions, ranging from ^{12}C to ^{40}Ar, stopping in Ilford K-1 and K-2 nuclear emulsions were simulated and the radiosensitivity parameters for these detectors chosen so that the simulated tracks resemble best those actually recorded. The results of such calculations are shown in Fig. 14 and Fig. 15. Here, the direction of motion of particles is from left to right, all particles stopping at the rightmost edge.

From these track simulations follows an important message for microdosimetry. According to microdosimetric considerations, the response of a detector to heavy charged particles is determined by the shape of the spectrum of microdepositions of energy in spheres representing the sensitive sites of the detector. There is no reason to expect different microdepositions of energy in grains of nuclear emulsions of K-1 and K-2 stocks which differ only by ppm additions of sensitizing agents (usually gold) and by different development procedures, but not by size.

However, tracks of the same particles appear to be quite different in the two emulsions. Clearly, microdosimetry alone cannot predict the response of emulsions exposed to the same radiation field but developed differently (18).

A somewhat more realistic model of the photographic process assumes the existence of active centres, i.e. electron traps in the silver halide grains in the emulsion. Latent image formation may begin when free electrons become trapped in these centres. The number of active centres in each grain and their electron capture efficiency could strongly depend on the development procedure. In this context, the c-hit model would offer a better phenomenological description of nuclear emulsion properties than microdosimetry which would relate the effects only to the overall size of the silver halide grains in the emulsion.[1]

It appears that the K-1 emulsion is a 1-hit detector, while the K-2 stock is best fitted as a highly supralinear 8-hit detector.

[1] I am grateful to Dr. Lewandowski for this comment

The appearance of tracks of the same ions in each emulsion is quite different. One would perceive a "detection threshold" in the K-2 emulsion, which in fact appears as such only because of the more rapid appearance of developed grains against a background of randomly blackened single grains, compared with the "linear" K-1 stock.

One should bear this argument in mind when discussing thresholds in radiobiology, or stochastic and non-stochastic effects. These concepts are most likely based on an incorrect perception of a rapid "supralinear" onset of an observed effect above a fixed background level.

General remarks

The track structure model presented here concerns physical detectors which are described by the c-hit target model. While three radiosensitivity parameters fully describe a physical detector, biological systems, such as mammalian cells, require four parameters to describe their survival or transformation RBE. This appears to be a phenomenological rather than a structural requirement.

A surprisingly broad range of physical systems has been successfully described by this model. Apart from those mentioned here (nuclear emulsions, enzyme and virus inactivation, the Fricke, thermoluminescence and alanine dosimeters), several other detectors, such as scintillators, dye-film dosimeters, photoresists or etchable track detectors have been studied (19). Most of these are described by 1-hit statistics of target inactivation, but multi-hit detectors have also been found.

What features of a detector make it amenable to a track theory calculation? Fading, repair or dose-rate effects are not explicitly incorporated in the theory. The theory assumes that dose is delivered to the sensitive target over a period which is short compared to the characteristic metastable time for the detector.

The theory assumes that the statistical character of target or sensitive site inactivation is adequately described by the c-hit or m-target models representing the average response of the detector to doses of test radiation averaged over the volume of the detector. Since the model also applies a radial distribution of dose averaged over the target volume, it follows that, in principle, no further insight is to be gained from studies of radiation damage specific to heavy charged particles over that due to electrons (delta-rays).

Clearly, the calibration of the detector by measuring its response to doses of test radiation and the subsequent use of the radial distribution of delta-ray dose, as well as the $Z^{*2}/\kappa\beta^2$ factor, provide us with a phenomenologically corect scaling for treating the response of detectors after heavy charged particle irradiation.

The four-parameter cellular version of track theory, discussed in the next lecture, is firmly based on the physical model of track structure. The success of this cellular model in describing RBE dependences in cells irradiated by heavy ions may indicate that physical processes of radiation damage rather than the subsequent biological effects should be primarily considered when constructing first-order models of RBE in radiobiology. Hence, most of the general observations pertaining to effects of track structure in physical systems discussed in this lecture, should be applicable to radiobiology.

Introduction

In my first lecture I discussed track structure theory as applied to physical detectors, i.e. to detectors whose response to X and gamma radiations can be described by the c-hit model. Once the three radiosensitivity parameters (c - "hittedness", D_o - characteristic radiosensitivity, and a_o - the radius of the sensitive site) are established for a physical detector, the theory allows us to calculate the response (cross-section) for any charged particle irradiation, specified by its charge (Z), velocity (β) and fluence (F particles per cm^2). By introducing the kappa parameter to describe the detector and Z^{*2}/β^2 to describe the radiation, we were able to characterize the appearance of particle tracks (whether actually visible or not) in the detector by the product $Z^{*2}/\kappa\beta^2$. The transition between grain-coincident and track-width (or saturation) effects is at about $Z^{*2}/\kappa\beta^2 = 4$, followed by a further increase in the cross-section and, eventually, thindown at higher values of $Z^{*2}/\kappa\beta^2$.

Most of the c-hit detectors discussed were 1-hit detectors whose response to X and gamma radiations was linear (exponential) and whose relative effectiveness to charged particle irradiations never exceeded 1, as represented by curve 5 in Fig. 13.

Most cellular systems behave quite differently.

A typical response of a cellular system where survival is the biological endpoint, is shown in Fig. 16, quoted from a textbook on radiobiology (20). The dose dependence of the surviving fraction after X-ray irradiation, plotted in semi-logarithmic coordinates, is a shouldered curve. After irradiation with fast cyclotron neutrons this dose dependence becomes steeper and purely exponential (shoulderless). The radiobiological effectiveness (RBE) of fast neutrons, which is the ratio of X-ray and fast neutron doses required to achieve the same given level of survival, is seen to be greater than 1 and to increase with increasing level of survival (or decreasing doses).

In fact, when survival curves are studied after a variety of charged particle irradiations, one observes a gradual transition from shouldered to purely exponential shapes, as shown in Fig. 17, where bacterial spores under anoxic conditions were irradiated with heavy ions ranging from protons to fluorine (Powers et. al, 1968, quoted after (4)). The general trend is that at a given survival level, RBE is observed to increase with the LET of the bombardment up to a maximum around 100 keV/um and then to decrease, as shown, e.g., by curve 1 or curve 2 in Fig. 13.

However, more accurate RBE-LET measurements show that RBE is not a univocal function of LET, as has been pointed out by Katz several years ago. This is clearly demonstrated in Fig. 18, where the highest values of RBE are observed for the lightest ion, He.

Any theory of RBE should provide an explanation of these experimental findings, at least in a phenomenological fashion. In this lecture I shall demonstrate that by incorporating a fourth independent parameter - the "saturation cross-section", σ_0, the track structure theory discussed in my first lecture can successfully describe cellular survival and neoplastic transformations in mammalian cells after charged particle irradiations. I shall also discuss the applications of this model to heavy ion beam radiotherapy, to evaluations of the low-dose radiation hazard, and the implications of the model to radiation protection.

The model

More extensive descriptions of the cellular track structure model developed by Katz and co-workers are given elsewhere (2-4). Here, I shall only present the main concepts of the model and discuss its equations shown in Fig. 19.

Let us first distinguish between "non-survival" (K) and "survival" (N/N_0) terms of eq.(1) in Fig. 19. Plots of m-target and c-hit forms shown in Fig. 4 represent the fraction of non-surviving objects (K), which increases with dose. An object (cell) can either not survive or survives, hence the relation is $K = 1 - N/N_0$. K will later be used to represent the number of transformed surviving cells in model calculations for neoplastic transformations in mammalian cells.

We say that a sensitive site in a detector or cell which exhibits c or m greater than one, requires more than one hit (e. g., a passage of an electron through its volume) for its (in)activation. Sites which have received less than the required number (c or m) of hits are "sublethally damaged" and do not contribute to the observed signal or biological endpoint (survival) until c hits are accumulated in the target, or until m sub-targets of the target are (in)activated.

Unlike 1-hit detectors, c-hit or m-target systems "remember" their sublethal damage. Their response after a given irradiation depends on their previous irradiation history, i.e. on the number of sublethally damaged targets at various stages of cumulative damage which now undergo further irradiation. Therefore, the response of c-hit or m-target detectors, to the test radiation, is supralinear when presented in the form of Fig. 4, or features a shoulder when

presented in the equivalent form of Fig. 16. The model names this mode of cell inactivation the gamma-kill mode. The gamma-kill mode survival probability, S_γ, after a dose D of gamma-ray test radiation is given by eq. (4) in Fig. 19.

The model also distinguishes the ion-kill mode of cell inactivation due to the passage of heavy ions. The ion-kill mode survival probability after a fluence F of heavy ions, S_i, is given by eq. (3) in Fig. 19. We recognize this formula from our discussion of the cross section in the previous lecture. The ion-kill mode of cell inactivation must yield purely exponential survival curves, such as the one shown in Fig. 16.

We require of the model that a gradual transition from shouldered X-ray (gamma-kill) to purely exponential (ion-kill) survival curves be possible, such as that shown in Fig. 17. The model achieves this by apportioning a part (Fig. 19, eq. (6)) of the ion dose D (eq. (10)) to the gamma-kill mode of inactivation. The single-particle activation cross-section is now approximated by the form $\sigma = (1 - \exp(-Z^{*2}/\kappa\beta^2))^m$ (see eq. (6)), a new parameter, σ_0, is introduced, the fraction P calculated as the ratio σ/σ_0, and the gamma kill dose given as (1 - P) D (see eqs. (5-6) in Fig. 19).

Let us now see how this formulation works in practice. For a very fast light ion (say, a proton), $Z^{*2}/\kappa\beta^2$ is small, therefore σ and $P = \sigma/\sigma_0$ are also small, so gamma-kill mode predominates. Survival curves after fast proton irradiation resemble those after X-ray doses, and the RBE of fast protons (see eqs. (8-10) in Fig. 19) is usually about 1. In the case of a slow heavy ion where $Z^{*2}/\kappa\beta^2 > 4$, there is saturation, P is about 1, ion-kill prevails, and RBE may exceed 1. RBE goes through a maximum when contributions from ion-kill and gamma-kill are about equal, i.e. at $Z^{*2}/\kappa\beta^2$ of about 2, or P = 0.5. As $Z^{*2}/\kappa\beta^2$ increases further above 4 into the track width region, the ratio σ/σ_0 also increases above 1 and finally decreases due to thindown. The value of σ_0 is so chosen that at saturation the measured value of cross-section matches the theoretical one. The kappa parameter is so chosen that the maximum value of RBE occurs at the observed value of Z^{*2}/β^2.

An impressive demonstration of a model fit to experimentally measured cross sections for inactivation of Chinese hamster cells is shown in Fig. 20. Here, E_0 (equal to D_0 of the first lecture), a_0 and κ are listed explicitly, as well as $\kappa = E_0 a_0^2 / (2\times10^{-7}$ erg/cm). Extrapolated cross-sections are measured experimentally from the exponentially decreasing parts of the shouldered survival curves[1] observed for ions of low Z^{*2}/β^2. Also, a modified form of the radial distribution of dose was used in these calculations in

[1] The point of intersection of the tangent to that part of the survival curve with the ordinate is called the extrapolation number (equal to m in the m-target model X-ray survival curve)

which the maximum range of the delta rays was divided by a factor of 5 (21).

Let us now recapitulate the description of the cellular model: The model requires the knowledge of four radiosensitivity parameters, two of which (m, the number of targets per cell and E_0, the characteristic X-ray dose) are extracted in principle from the response of the system to X-ray and ^{60}Co radiations. The remaining two (σ_0, the "plateau" value of the cross-section at the onset of the track-width regime, loosely interpreted as the cross-sectional area of the "container" for the inactivation sites, and k, a measure of the size of the inactivation site itself) are found in principle from survival measurements after track segment irradiations by energetic charged particles. In practice, all four parameters are fitted simultaneously to the entire set of data.

To accomodate for the capacity of cells to accumulate sublethal damage, two modes of inactivation are identified, namely ion-kill (or "intra-track") and gamma-kill (or "inter-track"). Cells inactivated by the passage of a single heavy ion are said to be inactivated in the ion-kill mode with inactivation cross-section σ whose value is less than σ_0 in the grain-count regime and greater than σ_0 in the track width regime. The fraction of track segments inactivating cells in the ion-kill mode in the grain-count regime is taken to be σ/σ_0 which is equal to P, the probability for inactivation in the ion-kill mode. P also approximates the fraction of dose deposited in the ion-kill mode. The RBE goes through a maximum when P is about 0.5. Cells not inactivated in the ion-kill mode can be sublethally damaged by the δ-rays from the passing particle and then inactivated, in the gamma-kill mode, by cumulative addition of sublethal damage due to δ-rays from other passing ions. Survival in the gamma-kill mode is taken to follow the m-target statistics of inactivation by secondary electrons from X-ray or gamma-ray photons.

Radiosensitivity parameters for survival were found by Roth, Sharma and Katz (3) for all biological systems for which experimental heavy ion data were published. A list of best-fitted values of these parameters is given in Fig. 21 (2). Representative values of the four parameters (e.g., for aerated T-1 human kidney cells) are m = 2.5, E_0 = 4.6 Gy, $\sigma_0 = 5.4 \times 10^{-7} cm^2$ and k = 1400 . We note that the difference between radiosensitivity parameters describing the same cell line irradiated in aerobic (O_2) and anoxic (N_2) conditions is usually only in the value of E_0 (equal to about 1.6 Gy, for T-1 cells).

Heavy ion beam radiotherapy

Beams of charged particles can be more advantageous than photon or electron beams from the point of view of radiation therapy due to the accuracy with which the volume of interest may be irradiated, the increased dose (Bragg peak) at the residual beam range, and due to the more nearly equal inactivation of normally oxygenated cells and oxygen-deprived tumour cells (lower oxygen enhancement ratio, OER). This has been shown for some types of tumours treated with beams of fast neutrons, mainly at Hammersmith (cf.(20)), but also in Krakow (22). Extensive radiobiological studies of beams of energetic (200 - 500 MeV/amu) He, C, Ne, Ar and Fe ions have been performed at Lawrence Berkeley Laboratory (for references, see (23 - 26)), in anticipation of heavy ion therapy. A brief review of some of the work of Katz and collaborators (24-26) should demonstrate the potential usefulness of the cellular track structure model in heavy ion beam radiotherapy.

Using a relatively simple beam model in which primary, secondary and tertiary products could be generated and the cellular track theory calculations performed for these products, the measured dose-depth distributions and survival curves measured for T-1 kidney cells at different beam depths could be reproduced quite adequately (26). Examples, for a 594 MeV/amu Ne beam, are shown in Fig. 22 and Fig. 23.

Since the width of the Bragg peak is insufficient to irradiate a tumour uniformly, the beam is dispersed in incident energy by a suitably designed ridge filter which disperses the Bragg peak over a range of about 5 cm (for details, cf. (24-26) and references therein). An example of a calculated dose-depth curve for a filtered 429 MeV/amu Ne beam is shown in Fig. 24.

Survival levels v. depth for aerobic T-1 human kidney cells after three different filtered 429 MeV/amu Ne beam fluences are shown in Fig. 25. From the results of fast neutron therapy at Hammersmith one may infer (24,25) that the dose after which 25 - 40% normal cells (represented by aerobic T-1 human kidney cell parameters) survive in the tumour region after a single fraction, is clinically acceptable from the point of view of skin reaction and early response of the irradiated tumours. It would therefore appear that, for the exemplary filtered Ne beam, a fluence 2.5 x 10^7particles/cm^2, the central survival depth-curve in Fig. 25, would be acceptable. However, cells in different organs may have different radiosensitivies (represented in the model by sets of different cellular parameters) which will lead to different survival-depth curves after the same beam dose (fluence), as shown in Fig. 26. An additional complication is the very non-homogeneous depth distribution of RBE, shown at 10% survival for aerobic and anoxic T-1 cells irradiated by the same filtered 429 MeV/amu Ne beam, in Fig. 27.

Given the possibility of performing depth-survival calculations using radiocellular parameters representing aerobic (normal) and anoxic (presumably tumour) cells which best represent the radiosensitivity of the cells irradiated *in vivo* in a clinical situation for a variety of heavy ion beams, how do we optimize our choice? First, we assume that the clinical constraint is 30% survival of normal (aerobic) cells after each dose fraction. Next, we may study the anoxic-aerobic survival ratio in the tumour region as an indication of the possibility that oxygen-deprived tumour cells may survive the treatment schedule. Thirdly, we may want to optimize the surviving fraction, N/N_0, of normal (aerobic) cells at the skin surface. Clearly, we would wish both the second and third parameters to be as close to unity as possible, but there is yet no clear clinical guidance as to the priority of any one of these considerations (24,25).

On the basis of these factors there is however a clear advantage of double-port[1] over single-port irradiation. This is illustrated in Fig. 28, where the dose-depth curve is calculated, again for the exemplary 429 MeV/amu filtered Ne beam, in Fig. 29, where a high and constant anoxic-aerobic survival ratio resulting from a flat distribution of RBE is expected over the tumour region, and in Fig. 30, where high skin sparing is predicted.

Thus, even though technically more complicated, double-port heavy ion beam irradiation facilities should offer definite radiotherapeutical advantages over the single-port installations used presently (24-26).

It would also appear that the knowledge of the biological effect of the planned treatment rather than just the dose distribution over the region of interest, should be helpful to the radiotherapeutist. Track structure calculations offer this possibility.

There is no conceptual difficulty in applying the same model calculations to fast neutron beam radiotherapy, provided that suitable neutron transport codes giving the energy spectra and fluences of secondary charged particles are available, and that realistic cellular radiosensitivity parameters corresponding to given radiotherapeutic situations are suitably selected.

Neoplastic transformations in mammalian cells

Cell cultures are the best systems for evaluating the diverse biological effects of radiation at a cellular level. As reflected in the course of this lecture, cellular survival has up to now

[1] Two identical antiparallel beams acting simultaneously

been the most extensively studied biological endpoint[1]. With the development of cell culture techniques , studies of neoplastic transformations in mammalian cell cultures became possible (for a review, see Borek (27)). A widely used system is the C3H10 T1/2 cell line originating from mouse embryos. Results of a systematic study of survival and neoplastic transformations in this cell line after irradiation with heavy ions accelerated at the BEVALAC facility have been published recently by Yang et al. (28). Using this data set, we made the first attempt at fitting track structure theory parameters for neoplastic transformations in the C3H10T1/2 cell line (9).

The response of a cell culture in vitro could be representative of in vivo effects, hence knowledge of radiocellular parameters for transformations could lead to insights concerning cancer induction in man, especially at low doses. This point will be discussed later.

Yang et al. (28) also investigated the repair capacity of cells after heavy ion and X-ray irradiations by plating exposed cells either immediately after irradiation or by delaying plating by 24 hours, to allow for cellular repair. They found that transformation lesions induced by heavy charged particles may not be repairable.

To evaluate transformation frequency per surviving cell, Yang et al. assessed independently survival and transformation for a range of beam particle fluences. They then calculated transformation RBE values for each heavy ion irradiation at an X-ray dose at which 50% cells survived.

From Yang's reported survival data (28) shown in Fig. 31, by simultaneously fitting to all data points, we found (9) the following survival radiosensitivity parameters : $m = 3$, $\kappa = 750$, $\sigma_0 = 5 \times 10^{-7} cm^2$ and $E_{0,inst} = 1.7$ Gy for cells plated immediately after irradiation (instantaneous plating), and $E_{0,del} = 2.8$ Gy for cells plated 24 hours after irradiation (delayed plating). A comparison between the measured (28) and calculated (9) RBE values, at 10% surviving fraction, for cells plated immediately after irradiation, is shown in Fig. 32. The overall agreement between theory and experiment is within 15% or better. The multi-valuedness of calculated RBE-LET dependences is evident and would perhaps have been confirmed experimentally if another choice of beam energies were made. The values of fitted survival parameters are not very different from those found for survival of other mammalian cells (cf. Fig. 21).

---

[1] Results of investigations of mutations in plant cells (Underbrink and co-workers) and in cell cultures (Goodhead and co-workers) have not yet been incorporated in the model.

The transformation data (28), shown in Fig. 33, were much more difficult to interpret, due to the scatter of experimental data points. Transformation experiments are clearly difficult to reproduce. This becomes apparent when all the X-ray induced transformation dependences, which should all in principle be identical, are gathered on one plot, as shown in Fig. 34. Here, distinction between m-target models with m=2 or m=3 is difficult.

Over a range of possible assignments, the set: $m_T = 2$, $\kappa_T = 750$, $\sigma_{0T} = 1.15 \times 10^{-7}$cm,^{2} $E_{0T,low} = 180$ Gy and $E_{0T,high} = 260$ Gy reproduces the experimental data set well enough, including the measured RBE values, as shown in Fig. 35. In this figure data for both instantaneous and delayed plating are displayed, showing agreement to within 25% for all bombardments except Ar, and a "splitting" with LET similar to that for survival.

We note that the ratio of "container" diameters for cell inactivation and cell transformation in C3H10T1/2 cells ($(\sigma_0/\sigma_{0T})^{1/2}$) is about 60.

We accounted for the apparently increased radioresistance in survival and transformations of cells plated 24 hours after irradiation by modifying the value of E_0, in a manner employed earlier for calculating survival under aerobic and anoxic conditions (4).

The assumption uderlying our calculations is that the transformation and survival processes are independent of each other. While a cell that does not survive cannot become transformed, the assumption stipulates that the same fraction of transformed cells would be found in any sample of the original population, if such an assay could be made for cells that cannot form colonies. This assumption may be valid for a calculation describing the number of transformed cells per survivors, where the surviving fraction is reasonably high, say above 50%.

From our analysis of transformation after X-ray and high-LET irradiation of the C3H10T1/2 cell system we may conclude that a calculation of transformation frequency can be made for an arbitrary radiation environment, as long as dose-modifying factors, e.g. due to variation in dose rate or dose fractionation, can be ignored. On these premises, I shall now discuss model predictions for low-dose oncogenesis.

Implications for radiation protection

Let us now apply the cellular track structure model to the low-dose region of interest to radiation protection. In this discussion (10), I shall essentially follow the arguments of Katz and Hofmann (29) and of Hofmann, Zhang and Katz (30).

We note that cellular survival and transformation are described by sets of parameters with m ranging from 2 to 3.5. The model would therefore imply that extrapolation of radiation risk to low doses of X or gamma radiation is quadratic or even cubic, but definitely not linear. This conclusion is based on model fits to entire (heavy ion and X-ray) data sets rather than on analysis of X-ray data alone, and on the tacit assumption that the response of isolated cell cultures in vitro is representative of radiation oncogenesis in the human organism as a whole.

The model specifies the meaning of the low-dose region. For heavy charged particle radiations this is a region of doses where biological targets, such as cells or their components, are traversed only by individual particles, implying that effects of track overlap (gamma kill) can be neglected. Only ion kill needs to be considered.

A source of information on low-dose radiation oncogenesis is the study of excess lung cancers in populations exposed to enhanced levels of radon in the environment, and of cancers in the group exposed at Hiroshima and Nagasaki to the two American atom bombs (31-35).

Excess lung cancers in uranium miners have been studied in USA, Czechoslovakia and Canada. Recently, an assessment of the risk of total lung cancers has been made for a high background area and a control area in China, indicating that at low alpha energy exposures the excess risk of lung cancer may be lower than that predicted by the linear hypothesis (for references, see (30)).

The usually assumed linear estimate of the average cancer risk for different organs and types of radiation is 10 cancers per cGy and per 10^6 persons (31).

Let us assume that lung cancer risk follows from the radiation damage by low doses of alpha particles to lung tissues and represent the probability of cancer occurrence by a product of the probability of cell transformation and that of cell survival after a dose (fluence) of alpha particles, in the ion-kill mode. We take the probability of cancer occurrence F(D) to be proportional to the product of transformation probability $T(D) = 1 - \exp(- P_T \sigma_{oT} F)$ and survival probability $S(D) = \exp(- P_S \sigma_{oS} F)$, where the subscripts T and S refer to transformation and survival, respectively, and where $D = F L_{av}$ (cf. eq. (10) in Fig. 19), L_{av} representing the value of LET averaged over the range of the alpha particle. The radon daughter alpha particles are here represented by an alpha particle of energy 6.72 MeV, relative speed $\beta = 0.06$, and $L_{av} = 150$ keV/μ. For this bombardment, Z^{*2}/β^2 is about 1000. Representing cell transformation by the parameters established earlier for C3H10T1/2 cells in vitro ($m_T = 2$, $\sigma_{oT} = 1.15 \times 10^{-10}$ cm^2, $k_T = 750$) and cellular survival by those of aerobic T-1 kidney cells ($m_S = 2.5$, $\sigma_{oS} = 5.4 \times 10^{-7}$cm^2, $k_S = 1400$), we find,

using eq.(5) in Fig. 19, $P_T = 0.59$ and $P_S = 0.22$. We are then able to calculate the product $F(D) = T(D) \times S(D)$.

If, after Jacobi (quoted by Hofmann, Katz and Zhang (30)), the excess lung cancer (LC) data is plotted as excess LC-risk per 10^6 person years as a function of potential alpha energy exposure in WLM, then the form $f_1 F(D)/D$ should be compared with the data. The proportionality constant f_1 (= 5.77×10^{6}) is chosen so that at 200 WLM the calculated excess risk is equal to 10 excess cancers per 10^6 person years, the exposure-dose conversion factor being 0.5 cGy/WLM (30). The comparison is made in Fig. 36. We note that in this representation, a linear risk hypothesis is represented by a horizontal line. The linear risk factors postulated by UNSCEAR (32), BEIR-II (33) and by Evans (34) are indicated in the figure. We also note that our calculation suggests a decreased hazard per WLM at higher exposures, due to the onset of cellular inactivation, which limits the number of cells able to transform and proliferate (i. e., potentially carcinogenic, in our interpretation).

There is a very considerable numerical discrepancy in our calculation. If we take the average volume of a radiation-sensitive organ in man to be 10 cm^3, it would contain about 10^9cells/cm^3 x 1000 cm^3 = 10^{12} cells. Allowing that each cell in the organ be exposed to alpha particles, and that at least 100 cells have to transform in order for a cancer to develop (9), our calculation, which numerically applies to a <u>single</u> cell, overestimates the hazard by any factor in the range 10^8 - 10^{10}. This observation is supported by other considerations, e.g. by those of Mole (35), who based his estimate of the risk factor on an assessment made for Nagasaki bomb survivors (see also Katz and Hofmann (29)). A possible way to resolve this discrepancy is to assume that cancer induction is a "multicellular" event (35,36) involving two (or more) adjacent cells. We shall represent a "two-cell" process by the form $F(D) = f_2 (T(D))^2 \times S(D)$, where the symbols retain their former meaning. The plot of this functional dependence, in the form $f_2 \times F(D)/D$, is also shown in Fig. 36. Again, the curve is normalized at 200 WLM, by choosing $f_2 = 2.05 \times 10^{10}$.

Apart from a somewhat better numerical adjustment, the quadratic-exponential form appears to offer a better fit to the data below 100 WLM, though, clearly, one is not able to resolve this issue conclusively.

Both the linear and quadratic forms suggest a decrease in hazard per WLM above 500 WLM. This is to be expected if only surviving cells can transform. At higher exposures, fewer surviving cells are available for subsequent transformation. In our interpretation, the probability of lung cancer incidence should decrease. Incidentally, the same argument applies to cancer radiotherapy; radiotherapy would hardly be effective if cellular

tranformations were more likely than cell inactivation, at radiotherapeutical dose levels.

The model thus supports a quadratic (rather than a linear or linear-quadratic) extrapolation to low X and gamma doses, the likelihood of a "multicellular" nature of oncogenesis, and suggests a decrease of radiation risk at higher doses if neoplastic transformations in cell cultures in vitro are to be representative of cancer induction in vivo. It is suggested on theoretical grounds that the UNSCEAR linear estimate may be excessively high at exposures below 20 WLM.

The model also suggests that for sufficiently high LET values every cell whose nucleus is traversed by a charged heavy particle is inactivated, thus eliminating the possibility of cell transformation. It would then follow that the recommended ICRU/ICRP quality factor used in radiation protection should tend to zero at the highest values of LET. Hofmann and Katz (37) proposed that quality factor Q be multiplied by the term $1-(1-\exp(-Z^{*2}/L/\beta^2))^m$, where the values of m and k were taken, e.g., from T-1 human kidney cell parameters. This would make the quality factor tend to zero above LET values of 500 keV/um and decrease its presently recommended maximum constant value of 20 above 175 keV/um to a maximum of about 10 around 100 keV/um. This proposal has been contested by Goodhead (38).

Controversies around the model - physical and biological factors

The track structure theory, or Katz's model, has been criticised mainly on radiobiological grounds. The physical basis of this model, presented in my first lecture, has often been overlooked in this criticism. In its interpretation of c-hit physical detectors, the model makes ad hoc use of several physical concepts (such as the radial distribution of dose, electron slowing-down spectrum, delta-ray production, etc.) without their proper justification or supporting physical data, such as measurements of appropriate doubly differentiated cross-section for the interaction of electrons with matter. This physical data are presently lacking, and the model suggests the most appropriate avenues for basic research related to the understanding of radiation damage in physical and biological systems. Development of c-hit detectors, such as "pure" 2-hit TLD materials, could further test the phenomenological correctness of the model as applied to physical systems. The evident success of the model in describing the response of 1-hit detectors should be exploited in refining detailed physical interpretations of radiation effects in the different detector media.

The main shortcoming of the model is in its inability to

incorporate time-dependent processes, such as cellular repair and the related dose-rate effects on cellular survival curves. Correcting the model in this aspect could involve modifying the formulation of the gamma-kill term by making E_0 time- or dose-rate -dependent and would introduce at least one more phenomenological parameter. Most radiobiologists agree that biological lesions after heavy charged particles (corresponding to ion-kill, in the model) are not easily repairable. The manner in which the values of radiosensitivity E_0 and extrapolation number m changes with X-ray dose rate is shown in Fig. 37.

The number and the meaning of the parameters of the cellular track model has often been questioned (see, e.g. Alper (39,40)). The model makes no claims other than being a purely phenomenological description, the success of which should be judged solely on the quality of its quantitative predictions. Unlike in some other models, the parameters of Katz's model are clearly specified, its mathematical structure is straightforward and its predictions are falsifiable. It is perhaps too early to identify the parameters of the model with biological structures (e.g., identifying the "bean-bag" with the cell nucleus, or the "beans" with elements in the cellular membrane or in the DNA complex) before the biological concepts of radiation damage mechanisms become clearer. It is difficult to imagine that the number of "beans" m should depend on the X-ray dose rate, as Fig. 37 would imply. The model strongly suggests, however, that sites connected with cell transformation are either different (of smaller size) than those related to cell killing, or that significant biological factors (such as "time windows" or "multicellular effects") are involved in cellular transformation.

The model makes extensive use of the hit concept which has a long tradition in radiobiology. In this context, three parameters (c or m,E_0, and a_0) are insufficient to generate RBE larger than 1 (see, e.g., the discussion in Gunther and Schulz (41)). This is the essence of "Katz's theorem" (15) concerning the RBE for 1-hit detectors, quoted in my first lecture. In fact, as pointed out by Alper (39,40), a number of biological systems violate this theorem; despite exponential survival curves after X-ray doses, RBE > 1 has been measured. Katz (15) questions the reliability of these observations.

A less serious concern is that the track structure model implies RBE values tending to infinity at low doses. This follows from representing X-ray survival by the m-target model whereby the mathematical form of the survival curve has zero initial slope. In fact, as illustrated in Fig. 38, survival curves with zero initial slope have been observed, despite the experimental difficulty of accurately measuring survival at very low doses. The issue is more likely a conceptual one, as RBE relying on dose-averaged quantities may have limited validity at truly low doses involving individual particle tracks.

There is a number of biological phenomena, such as individual variability of cellular radiosensitivity within groups of cells, even in an in vitro culture, or throughout the cell age cycle (Fig. 39), which are clearly beyond the scope of a simple phenomenological model based on physical principles. It is difficult to judge the relative importance of such effects. In biology, unlike in physics, first-order and second-order effects cannot be readily distinguished.

It clearly follows from track structure considerations that specification of radiation quality is possible only in strict relation to the properties of the detector. Hence, the usefulness of ion dose, LET, Z^{*2}/β^2 or any other combination of radiation field parameters is at best limited if not accompanied by the specification of the parameters of the detector. In this sense, there has been unjustified preoccupation with RBE-LET, QF-LET, or average LET dependences in radiobiology, radiotherapy and radiation protection. There appears to be no easy way out; the full physical specification of the radiation field in terms of ion charge, velocity and fluence, is mandatory. Perhaps up to now the uncertainty in distinguishing between the "radio-" and "biological" terms in radiobiology has obscured this point.

Track structure theory offers a reasonably clear distinction between the physical and biological aspects of radiation damage. It should therefore continue serving us as one of the theoretical guidelines in these investigations.

Acknowledgements

I have liberally quoted from work performed at Dr. Katz's Track Physics Laboratory at Lincoln, NE, USA, wherever possible from work I had participated in myself. I am grateful to Dr. Robert Katz for the numerous discussions of various aspects of his model, and to the IAEA (Vienna) for sponsoring my Fellowship at Lincoln.
I am grateful to Dr. William L. Mclaughlin (National Bureau of Standards, Washington, D.C.), to Dr. John W. Baum (Brookhaven National Laboratory) and to Dr. Johen Booz (Institut fur Medizin, Juelich) for inviting me to give these lectures at their institutions and for sponsoring my visits.
I wish to thank Dr. Zbigniew Lewandowski (INP) for helpful comments with regard to the text of these lectures

In the selection of material for this presentation, I have strived to present the concepts of the model rather than the complete theory. If I have failed, I have only myself to blame.

Literature

1. J.J. Butts and R. Katz. Theory of RBE for heavy ion bombardment of dry enzymes and viruses, Radiat. Res. 30, 855-871 (1967).

2. R. Katz, S. C. Sharma and M. Homayoonfar, The structure of particle tracks, in Topics in Radiation Dosimetry, F. H. Attix Ed., Academic Press, New York (1972).

3. R. Katz, Track structure theory in radiobiology and in radiation detection, Nucl. Track Detection 2, 1-28 (1978).

4. R. A. Roth, S.C. Sharma and R. Katz, Systematic evaluation of cellular radiosensitivity parameters, Phys. Med. Biol. 21, 491-503 (1976).

5. M. P. R. Waligórski, R. N. Hamm and R. Katz, The radial distribution of dose around the path of a heavy ion in liquid water, Nucl. Tracks Radiat. Meas. 11, 309-319 (1986) Int. J. Radiat. Appl. Instrum.,Part D.

6. M. P. R. Waligórski, Kim Sun Loh and R. Katz, Inactivation of dry enzymes and viruses by energetic heavy ions, in print, Int. J. Radiat. Appl. Instrum. (1987).

7. R. Katz, G. L. Sinclair and M. P. R. Waligórski, The Fricke dosimeter as a 1-hit detector, Nucl. Tracks Radiat. Meas. 11, 301-307 (1986), Int. J. Radiat. Appl. Instrum., Part D.

8. M. P. R. Waligórski, G. Danialy, Kim Sun Loh and R. Katz, Response of the alanine dosimeter to charged particle and neutron irradiations, in preparation (1987).

9. M. P. R. Waligórski, G. L. Sinclair and R. Katz, Radiosensitivity parameters for neoplastic transformations in C3H10T1/2 cells, in print, Radiat. Res. (1987).

10. M. P. R. Waligórski, On the low-dose extrapolation of neoplastic transformations in a mammalian cell line - Implications for radiation protection, submitted to Kernenergie (1987).

11. M. P. R. Waligórski, R. Katz, E. Byrski, T. Sarna, M. Pasenkiewicz-Gierula and J. Knapczyk, Mixed field dosimetry in a cyclotron-produced fast-neutron cacer radiotherapy beam with special emphasis on a newly developed alanine system, in Proc. 4th Symp. on Neutron Dosimetry, Munich-Neuherberg, 1-5 April 1981, vol. 2, pp. 489-498.

12. M. P. R. Waligórski and R. Katz, Supralinearity of peak 5 and peak 6 in TLD-700, Nucl. Instrum. Methods 172, 463-470 (1980); 175, 48-50 (1980).

13. R. N. Hamm, H. A. Wright, R. Katz, J. E. Turner and R. H. Ritchie, Calculated Yields and Slowing-down Spectra for Electrons in Liquid Water: Implications for Electron and Photon RBE, Phys Med. Biol. 23, 1149-1161 (1978).

14. Zhang Chunxiang, D. E. Dunn and R. Katz, Radial distribution of dose and cross-sectons for the inactivation of dry enzymes and viruses, Radiat. Protect. Dos. 13, 215-218 (1985).

15. R. Katz, High LET constraints on low LET survival, Phys. Med. Biol.,23, 909-916 (1978).

16. P. Schmidt, J. Fellinger, J. Henniger and K. Hubner, Determination of relative light conversion factors of TL detectors for high energy protons, Kernenergie 29, 239-341 (1986), and P. Schmidt, personal communication (1987).

17. T. E. Furtak and R. Katz, Simulation of particle tracks in emulsion, Radiation Effects 11, 195-199 (1971).

18. R. Katz, Particle tracks in emulsion: A message for microdosimetry, Proc. 7th Symposium on Microdosimetry, 8-12 Sept. 1980, Oxford UK, J. Booz, H. G. Ebert and H. D. Hartfield Eds., Harwood Academic Publishers, Brussels and Luxembourg 1981, vol. II, pp. 831-840.

19. R. Katz, S. C. Sharma and M. Homayoonfar, Detection of Energetic Heavy Ions, Nucl. Instrum. and Methods 100, 13-32 (1972).

20. Radiation Biology in Cancer Research, R. E. Meyn and H. R. Withers Eds., Raven Press, New York, 1980.

21. R. Katz, D. E. Dunn and G. Sinclair, Thindown in Radiobiology, Radiat. Prot. Dosim. 13, 381-284 (1985).

22. J. Skołyszewski, J. Huczkowski, E. Byrski, A. Chrzanowska, S. Korzeniowski, B. Łazarska, M. Reinfuss, K. Urbański and A. Michałowski, Clinical use of fast neutrons from the U-120 cyclotron in Kraków, Nowotwory 29, 169-177 (1979) (in Polish)

23. R. Katz, B. Ackerson, M. Homayoonfar and S. C. Sharma, Inactivation of Cells by Heavy Ion Bombardment, Radiat Res. 47, 402-425 (1971).

24. R. Katz and S. C. Sharma, Response of cells to fast neutrons, stopped pions and heavy ion beams, Nucl. Instrum. and Methods 111, 93-116 (1973).

25. R. Katz and S. C. Sharma, Heavy Particles in Therapy: An Application of Track Theory, Phys. Med. Biol. 15, 413-435 (1974).

26. R. A. Roth and R. Katz, Heavy Ion Beam Model for Radiobiology, Radiat. Res. 83, 499-510 (1980).

27. C. Borek, Radiation oncogenesis in cell culture, Advances in Cancer Research 37, 159-232 (1982).

28. T. C. Yang, L. M. Craise and C. A. Tobias, Neoplastic cell transformation by heavy charged particles. Radiat. Res. Suppl. 104, S-177 - S-187 (1985).

29. R. Katz and W. Hofmann, Biological effects of low doses of ionizing radiations: particle tracks in radiobiology, Nucl. Instrum. Methods 203, 433-442 (1982)

30. W. Hofmann, R. Katz and Zhang Chunxiang, Lung cancer incidence in a Chinese high background area - epidemiological results and theoretical interpretation, The Science of the Total Environment 45, 527-534 (1985).

31. National Academy of Sciences Committee on Biological Effects of Ionizing Radiation,The effects on populations of exposure to low levels of ionizing radiation: 1980 (BEIR III) National Academy Press, Washington DC 1980.

32. Ionizing Radiation: Sources and Biological Effects, United Nations Scientific Committee on the Effects of Atomic Radiations, 1977 Report to the General Assembly, with annexes, United Nations, New York, 1977.

33. National Academy of Sciences Committee on Biological Effects of Ionizing Radiation,The effects on populations of exposure to low levels of ionizing radiation: 1972 (BEIR II) National Academy Press, Washington DC 1972.

34. R. D. Evans, J. H. Harley, W. Jacobi, A. S. McLean, W. A. Mills and C. G. Stewart, Nature, 290, 98-100 (1980).

35. R. H. Mole, Dose-Response Relationships, in: Radiation Carcinogenesis: Epidemiology and Biological Significance J. D. Boice, Jr. and J. F. Fraumeni, Jr., eds., Raven Press, New York 1984.

36. H. Rossi and E. J. Hall, The multicellular nature of radiation carcinogenesis,in: Radiation Carcinogenesis: Epidemiology and Biological Significance, J. D. Boice, Jr. and J. F. Fraumeni,Jr.,eds., Raven Press, New York 1984.

37. W. Hofmann and R. Katz, Quality Factor for Low Doses of High-LET Radiations, Healt Phys. 44, 173-175 (1983).

38. D. T. Goodhead, Quality Factor for Low Doses of High-LET Radiations: Comments on the Proposal of Hofmann and Katz, Health Phys. 46, 237-239 (1984).

39. Cellular Radiobiology, by T. Alper, Cambridge University Press, Cambridge, London, New York, Melbourne, 1979.

40. T. Alper, The Inadequacy of Physical Models in Radiobio logy, in: Proc. 7th Symp. on Microdosimetry, Oxford UK, 8-12 Sept. 1980, Harwood Academic Publishers, Commission of the European Communities, Brussels and Luxembourg, 1981, vol. 2, pp. 1463-1474.

41. Biophysical Theory of Radiation Action, by K. Günther and W. Schulz, Akademie Verlag, Berlin, 1983.

Figure captions:

Fig. 1. Tracks of relativistic proton, nitrogen and calcium ions in Ilford G.5 emulsion. From (2), courtesy R. Katz.

Fig. 2. Stopping tracks of heavy ions in Ilford G.5 emulsion. Bragg peak occurs at a residual range from 4 (for Z = 7) to 20 (for Z = 26) um. From (3), courtesy R. Katz.

Fig. 3. Principle of determining the radial distribution of activation probability as a convolution of the function describing the activation probability for uniform "test" irradiation (panel 1) and the function describing the radial distribution of dose around the path of a heavy ion (panel ..). For other explanations, see text.

Fig. 4. The m-target (upper diagram) and c-hit forms used to represent detector response to doses of test radiation. A is the dose expressed in units of characteristic saturation dose D_0. From (3), courtesy R. Katz.

Fig. 5. The 1-hit response of alanine dosimeter to ^{60}Co doses. From (11).

Fig. 6. The response of TLD-700 to ^{60}Co doses represented as a composition of 1-hit and 2-hit detectors. From (12).

Fig. 7. Radial distribution of energy deposited around the path of protons of energies 1, 10,20, 50 and 100 MeV (full lines). Monte Carlo calculations (in liquid water) are presented as histograms. From (5).

Fig. 8. Measured radial distributions of dose, multiplied by the square of the radial distance and by β^2/Z^{*2}, for ions of 1 MeV/amu (uppermost group), 0.5 MeV/amu (central) and 0.25 MeV/amu (lowest group). Full line represents the presently used radial distribution of dose formula. From (5).

Fig. 9. Average dose, E(r), in sensitive sites of different radii calculated using the point-target radial distribution of dose formula of Fig. 7 and Fig. 8. Proton velocity, β = 0.99.

Fig. 10. Radial distribution of average dose in water, in "normalized coordinates", $Ea_0^2\beta^2/Z^{*2}$ v. t/a_0, where a_0 = 100 nm, for protons of velocities β = 0.05, 0.5 and 0.99.

Fig. 11. Radial distribution of average dose in water, in "normalized coordinates", $Ea_0^2\beta^2/Z^{*2}$ v. t/a_0, where a_0 = 1000 nm, for protons of velocities β = 0.05, 0.5 and 0.99.

Fig. 12. Measured and calculated cross sections for virus inactivation after heavy ion bombardment. From (6).

Fig. 13. Upper panel: RBE-LET dependences for some biological systems, lower panel: calculated relative efficiency of peak 5 and peak 6 in TLD-700, demonstrating the capability of supralinear detectors to mimic the response of biological systems to high-LET radiations. Curve 5 in the upper panel (T-1 phage in broth) would be representative of the response of 1-hit detectors. From (12).

Fig. 14. a) Stopping ^{40}A, ^{20}Ne, ^{16}O, ^{14}N and ^{12}C ions of initial energy 10.5 MeV/amu in Ilford K-1 emulsion; b) computer simulation of tracks of these ions, assuming this emulsion to be a 1-hit detector. From (3), courtesy R. Katz.

Fig. 15. a) Stopping ^{40}A, ^{20}Ne, ^{16}O, ^{14}N and ^{12}C ions of initial energy 10.5 MeV/amu in Ilford K-2 emulsion; b) computer simulation of tracks of these ions, assuming this emulsion to be an 8-hit detector. From (3), courtesy R. Katz.

Fig. 16. Survival curves for Ehrlich ascites cells irradiated with 250 kVp X-rays or cyclotron neutrons. The lines have been drawn by eye and the numbers to the right of the X-ray survival curve represent the RBE measured at the level of the arrows. From (20).

Fig. 17. Survival data for bacterial spores (anoxic) after irradiation with heavy ions, in comparison to theoretical curves generated by the four fitted radiosensitivity parameters. Also shown are the curves which would be generated by parameters bracketing 95% confidence limits (cf. table of parameters in Fig. 21). From (3), courtesy R. Katz.

Fig. 18. Relative biological effectiveness for survival of Chinese hamster cells as a function of LET. From Wulf et al., Radiat. Res. 104, S-122-S-134 (1985).

Fig. 19. Equations of the cellular track structure theory.

Fig. 20. Inactivation cross sections for Chinese hamster cells, an example of a theoretical fit to experimental data. Note the calculated ion-kill cross-section (full lines) first rising cubically in the grain count regime, saturating and rising further in the track width regime, and finally decreasing due to thindown. Broken lines are calculated values of the extrapolated cross-section. From (21),courtesy R. Katz.

Fig. 21. Celular radiosensitivity parameters, as fitted numerically to cell survival data. From (3), courtesy R. Katz.

Fig. 22. Calculated dose as a function of depth, compared to experimental data (open circles) for a 594 MeV/amu Ne beam. The energy chosen for the calculation (580.2 MeV/amu) gives best agreement between calculated and measured doses. From (26), courtesy R. Katz.

Fig. 23. Survival curves for T-1 human kidney cells in the neon beam of Fig. 22. The data, from Blakely et al., Radiat. Res. 80, 122-160 (1979), for hypoxic cells shown as open squares those for aerobically irradiated cells shown as solid squares. Lines are calculated from theory and the beam model. From (26), courtesy R. Katz.

Fig. 24. Dose-depth distribution for a single-port filtered 429 MeV/amu Ne beam calculated from the beam model (25). Courtesy R. Katz.

Fig. 25. Survival-depth distributions for T-1 human kidney cells, after different fluences (doses) from the beam of Fig. 24. Courtesy R. Katz.

Fig. 26. Survival-depth distributions for different cell lines after a fluence 2.5×10^7 particles/cm^2 from the beam of Fig. 24. Courtesy R. Katz.

Fig. 27. Depth distribution of RBE at 10% survival for anoxic (N_2) and aerobic (O_2) T-1 human kidney cells, for the beam of Fig. 24. Courtesy R. Katz.

Fig. 28. Dose-depth distribution for a double-port filtered 429 MeV/amu Ne beam (25). Courtesy R. Katz.

Fig. 29. Depth distribution of RBE at 10% survival for anoxic (N_2) and aerobic (O_2) T-1 human kidney cells, for the beam of Fig. 28. Courtesy R. Katz.

Fig. 30. Depth distribution of survival for anoxic (N_2) and aerobic (O_2) T-1 human kidney cells, for the beam of Fig. 28, at beam fluence 2.5×10^7 particles/cm^2. Courtesy R. Katz.

Fig. 31. Measured (28) and calculated survival fraction of C3H10T1/2 cells after irradiation with X-rays (X) and BEVALAC ions, for instantaneous (squares) and delayed (circles) plating. Above each box the ion and beam energy are given. Full lines represent model calculations using parameters listed in the figure. From (9).

Fig. 32. Measured (28) and calculated RBE at 10% survival, for C3H10T1/2 cells plated immediately after irradiation. From (9).

Fig. 33. Measured (28) and calculated transformation frequencies in C3H10T1/2 cells after irradiation with X-rays (X) and BEVALAC ions, for instantaneous (squares) and delayed (circles) plating. Above each box the ion and beam energy are given. Full lines represent model calculations using parameters listed in the figure. From (9).

Fig. 34. Measured (28) transformation frequencies in C3H10T1/2 cells after X-ray doses, for instantaneous (INST-upper abscissa) and delayed (DEL-lower abscissa) plating. Data are pooled from all experiments. Full line represents the m=2-target model ($E_{0,inst}$=180 Gy, $E_{0,del}$=260 Gy), broken line represents the the m=3-target model ($E_{0,inst}$=50 Gy, $E_{0,del}$=75 Gy). From (9).

Fig. 35. Measured (28) and calculated RBE for transformations in C3H10T1/2 cells at levels corresponding to 50% survival, for instantaneous (upper panel, upper right-hand ordinate) and delayed (lower panel, lower left-hand ordinate) plating. From (9).

Fig. 36. Excess lung cancer risk in uranium miners and total lung cancer risk in the inhabitants in high background areas in China vs. cumulative exposure to radon and thoron decay products in WLM. Theoretical curves are normalized to the same value at 200 WLM. Data points are taken from Hofmann, Katz and Zhang (29). From (10).

Fig. 37. Dependence of E_0 and extrapolation number n on the dose-rate for HeLa cells exposed to gamma rays in air. From (20).

Fig. 38. Fraction of CHO cells surviving various doses of ^{3}H-TdR, ^{125}I-UdR or external X-rays, plotted as a function of cumulative disintegrations per cell (left) or as a function of radiation dose (rad) to the cell nucleus (right). From R. L. Waters et al. Current Topics In Rad. Res. Quart. 12, 389-407 (1977).

Fig. 39. The age-response function for V79 cells and HeLa cells exposed to single doses of radiation. From W. K. Sinclair, Radiat. Res. 33, 620 (1968), after (20).

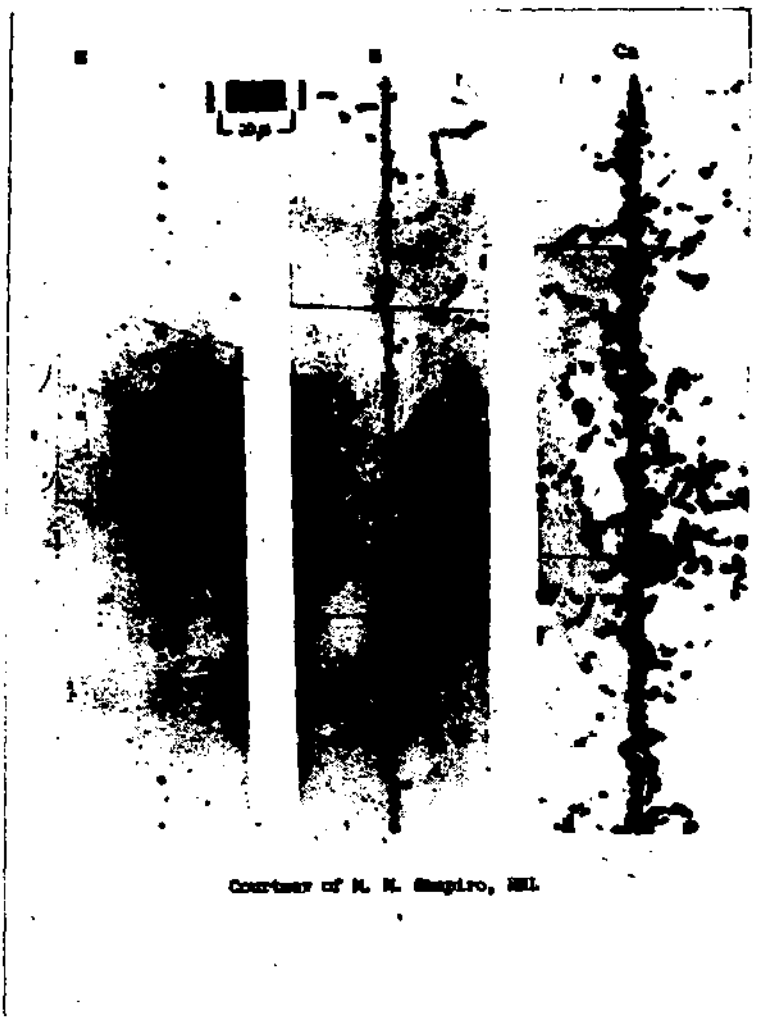

Fig. 1. Tracks of relativistic proton, nitrogen and calcium ions in Ilford G.5 emulsion. From (2), courtesy R. Katz.

Fig. 2. Stopping tracks of heavy ions in Ilford G.5 emulsion. Bragg peak occurs at a residual range from 4 (for Z = 7) to 20 (for Z = 26) um. From (3), courtesy R. Katz.

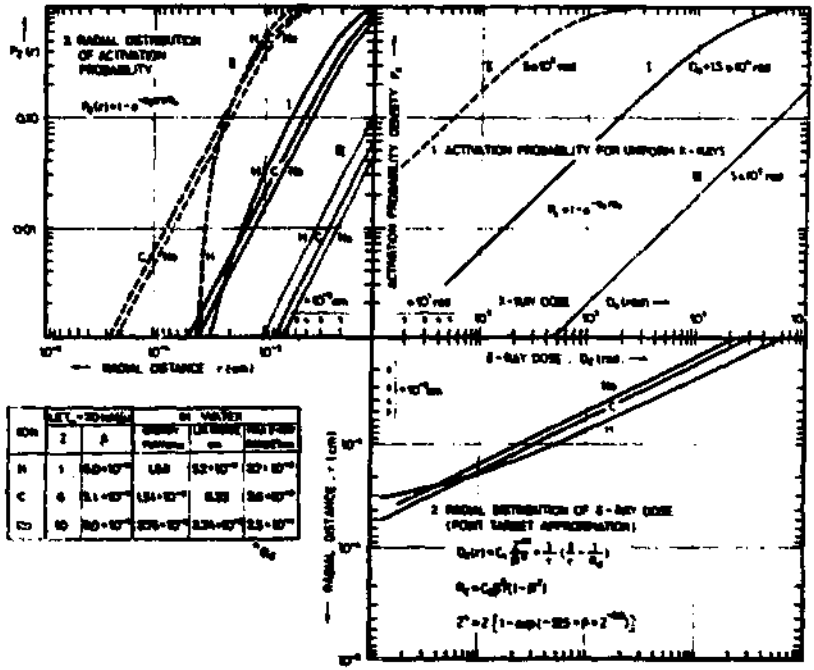

Fig. 3. Principle of determining the radial distribution of activation probability as a convolution of the function describing the activation probability for uniform "test" irradiation (panel 1) and the function describing the radial distribution of dose around the path of a heavy ion (panel 2). For other explanations, see text.

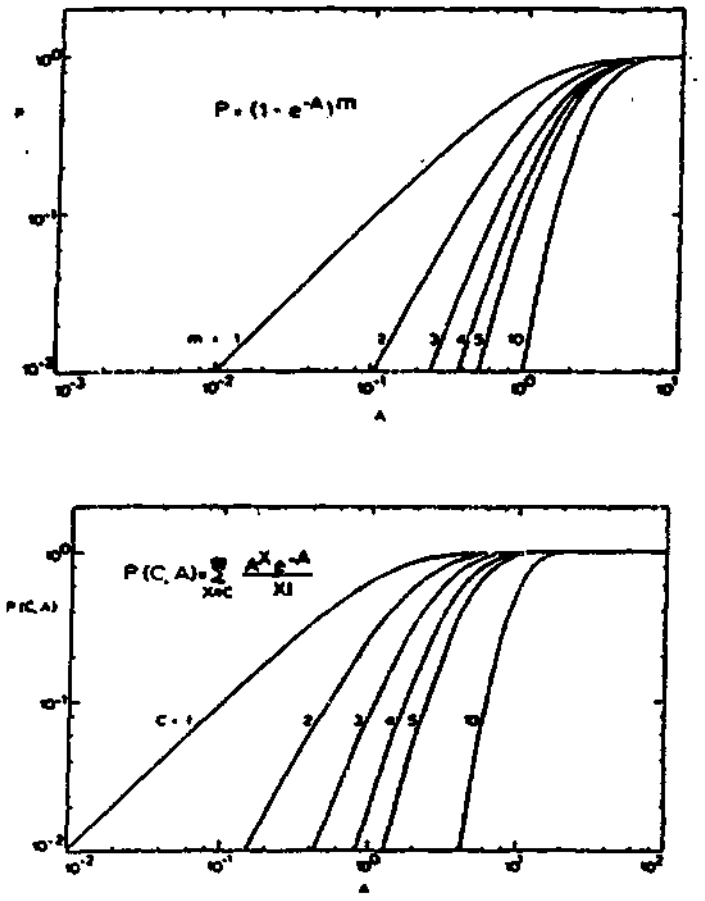

Fig. 4. The m-target (upper diagram) and c-hit forms used to represent detector response to doses of test radiation. A is the dose expressed in units of characteristic saturation dose D_o. From (3), courtesy R. Katz.

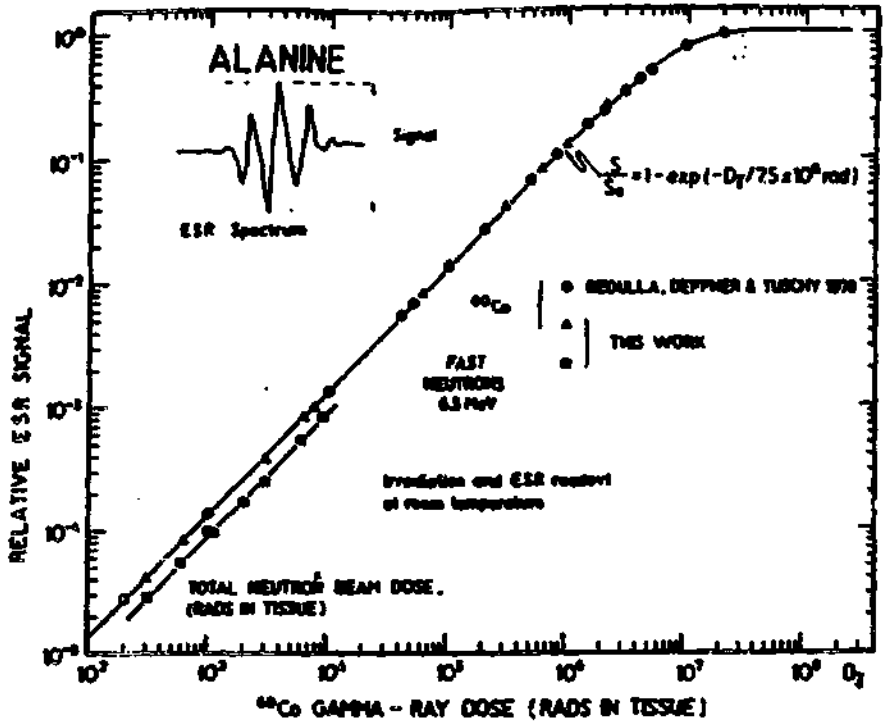

Fig. 5. The 1-hit response of alanine dosimeter to ^{60}Co doses. From (11).

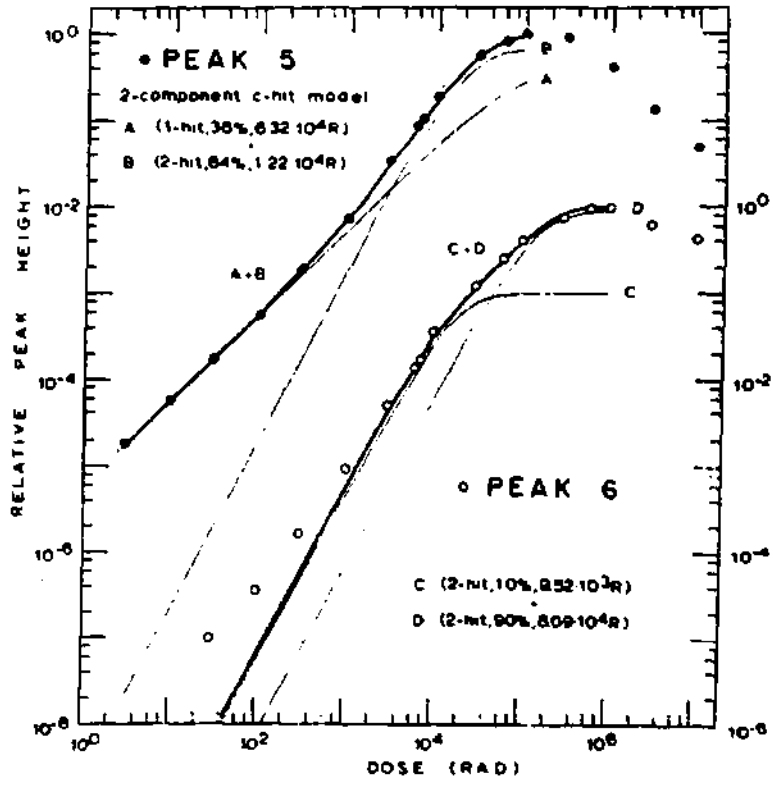

Fig. 6. The response of TLD-700 to ^{60}Co doses represented as a composition of 1-hit and 2-hit detectors. From (12).

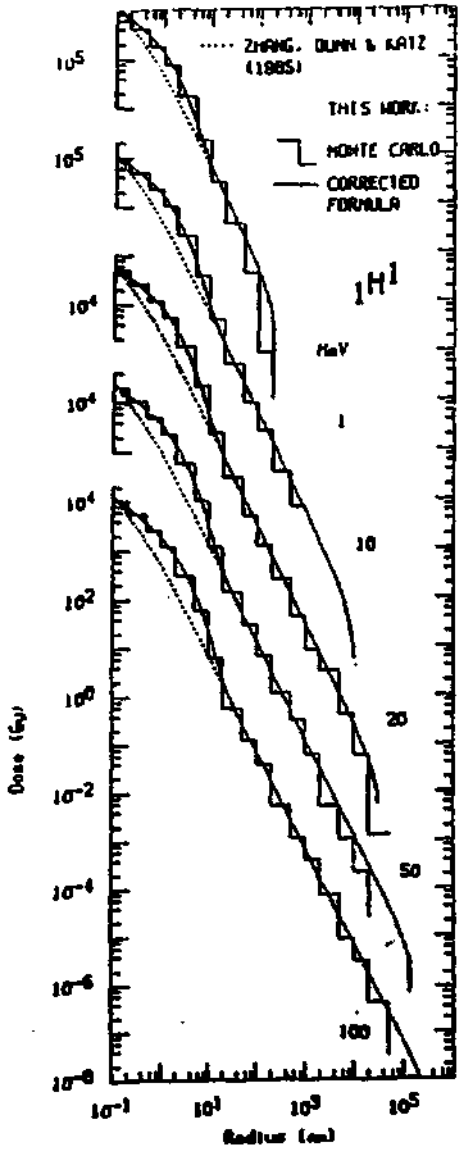

Fig. 7. Radial distribution of energy deposited around the path of protons of energies 1, 10,20, 50 and 100 MeV (full lines). Monte Carlo calculations (in liquid water) are presented as histograms. From (5).

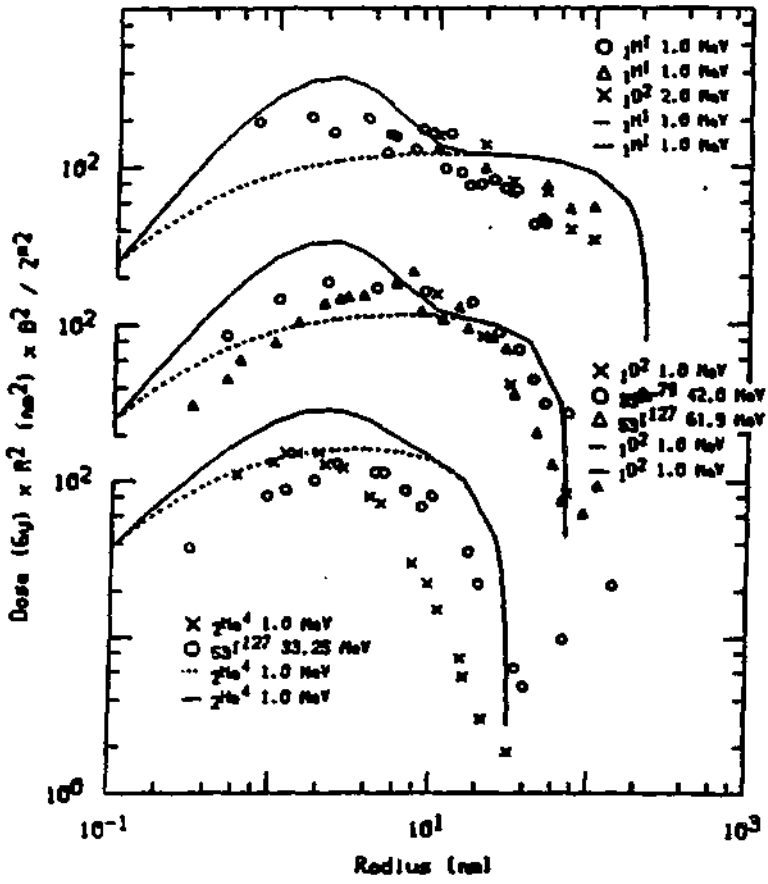

Fig. 8. Measured radial distributions of dose, multiplied by the square of the radial distance and by $\beta^2/2\pi e$, for ions of 1 MeV/amu (uppermost group), 0.5 MeV/amu (central) and 0.25 MeV/amu (lowest group). Full line represents the presently used radial distribution of dose formula. From (5).

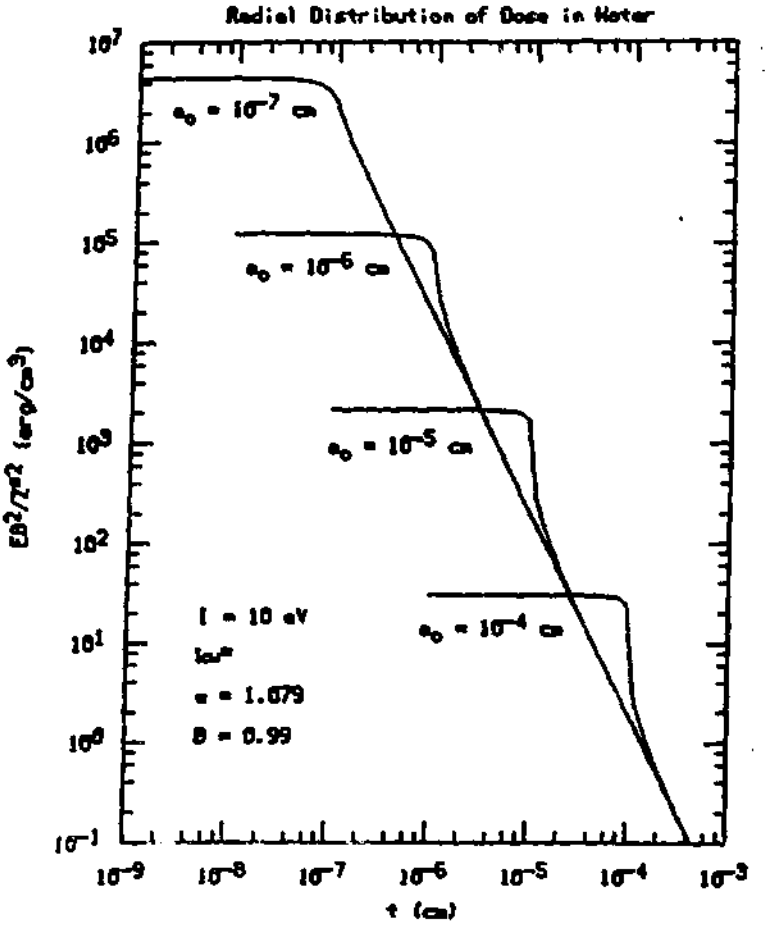

Fig. 9. Average dose, E(r), in sensitive sites of different radii calculated using the point-target radial distribution of dose formula of Fig. 7 and Fig. 8. Proton velocity, $\beta = 0.99$.

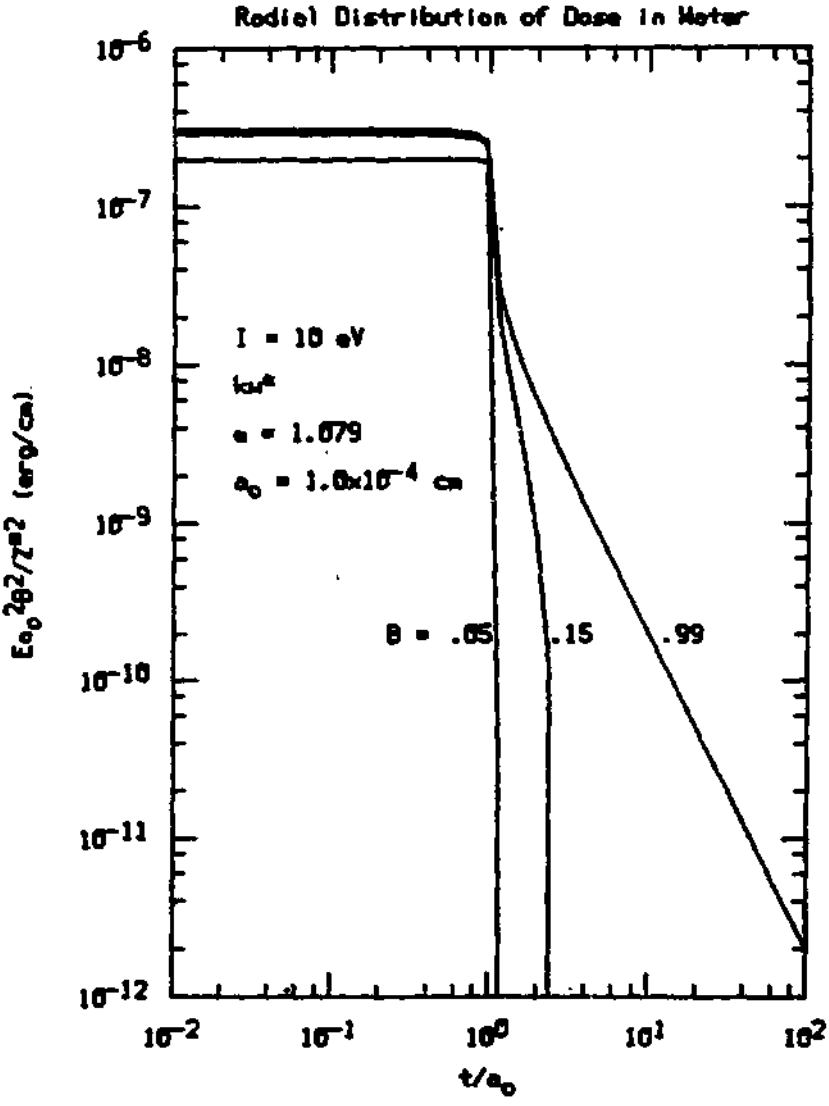

Fig. 10. Radial distribution of average dose in water, in "normalized coordinates", $Ea_0^2\beta^2/Z^{*2}$ v. t/a_0, where a_0 = 100 nm, for protons of velocities β = 0.05, 0.5 and 0.99.

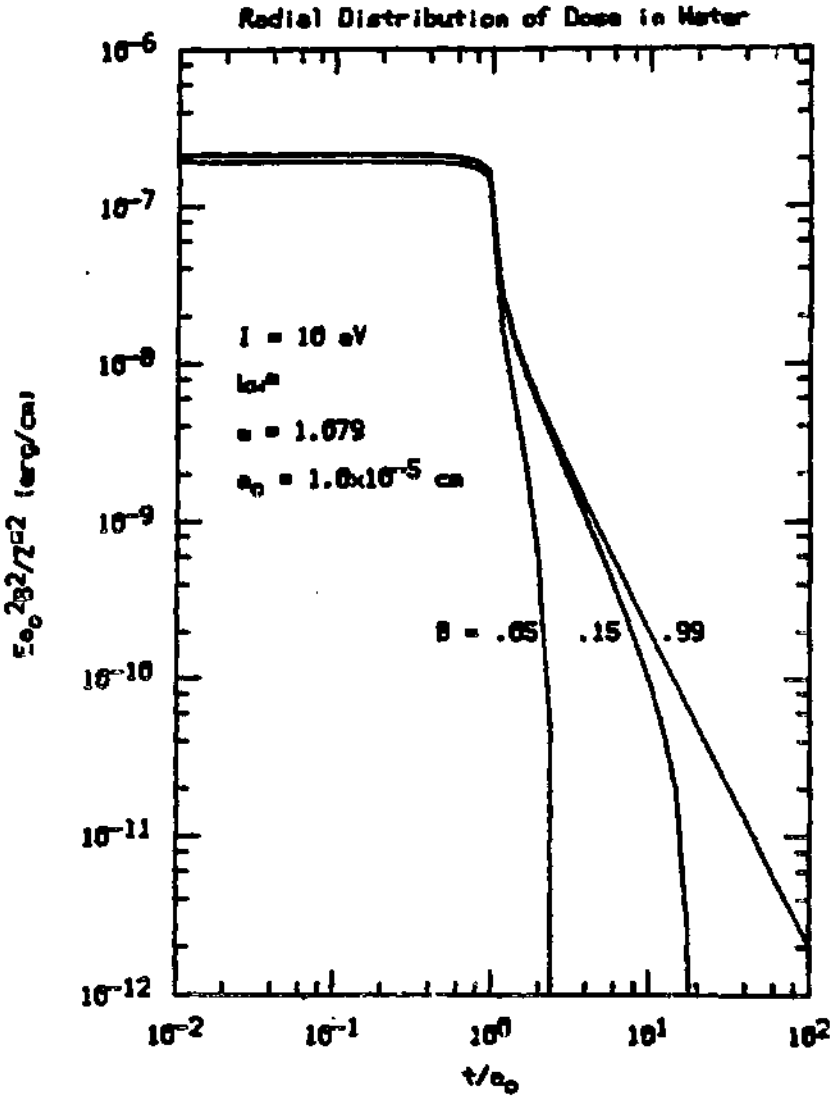

Fig. 11. Radial distribution of average dose in water, in "normalized coordinates", $Ea_0^2\beta^2/Z^{*2}$ v. t/a_0, where a_0 = 1000 nm, for protons of velocities β = 0.05, 0.5 and 0.99.

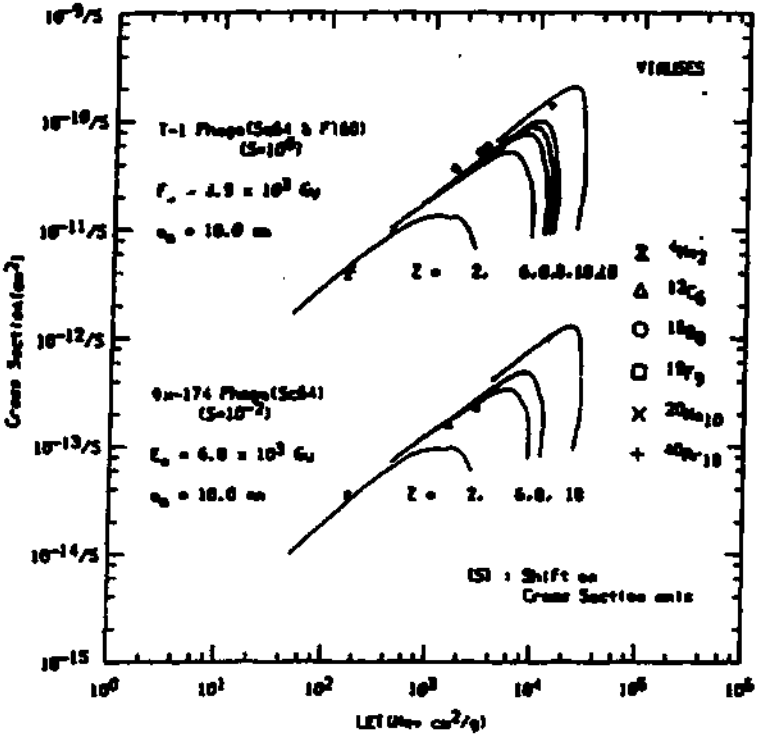

Fig. 12. Measured and calculated cross sections for virus inactivation after heavy ion bombardment. From (6).

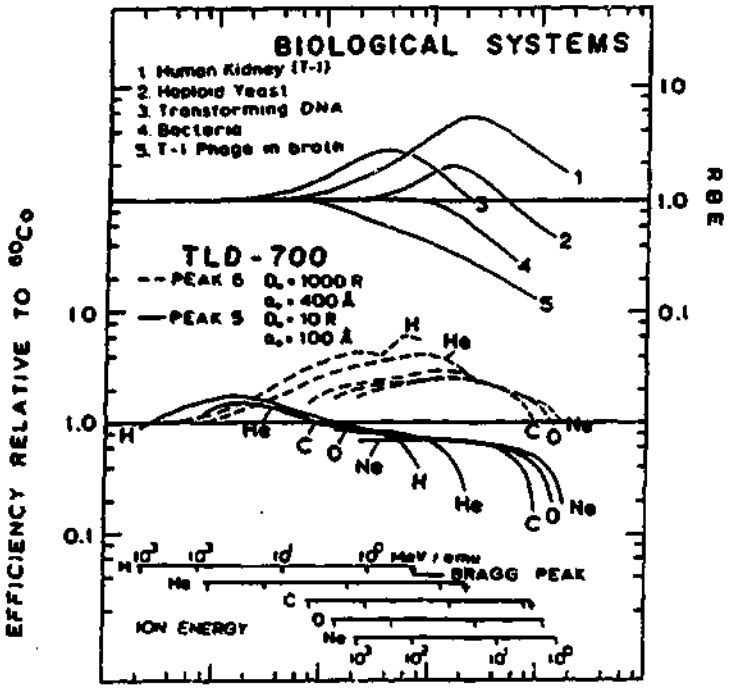

Fig. 13. Upper panel: RBE-LET dependences for some biological systems, lower panel: calculated relative efficiency of peak 5 and peak 6 in TLD-700, demonstrating the capability of supralinear detectors to mimic the response of biological systems to high-LET radiations. Curve 5 in the upper panel (T-1 phage in broth) would be representative of the response of 1-hit detectors. From (12).

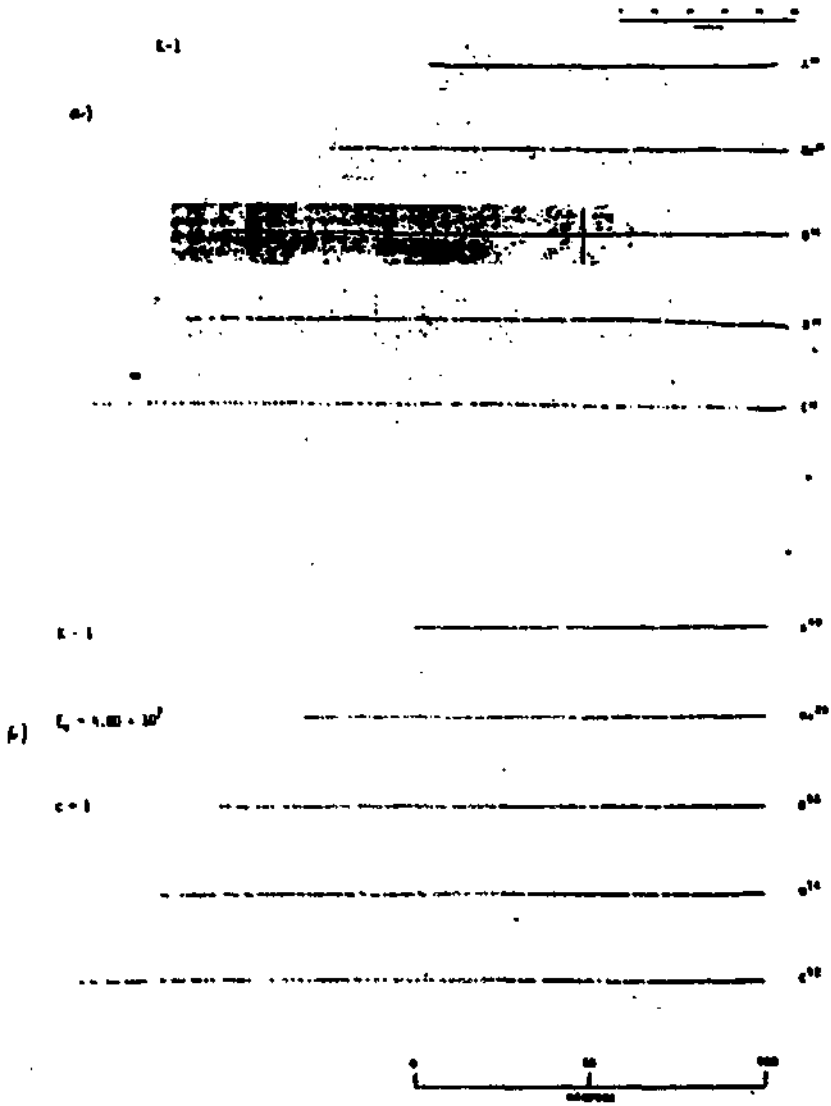

Fig. 14. a) Stopping ^{40}A, ^{20}Ne, ^{16}O, ^{14}N and ^{12}C ions of initial energy 10.5 MeV/amu in Ilford K-1 emulsion; b) computer simulation of tracks of these ions, assuming this emulsion to be a 1-hit detector. From (3), courtesy R. Katz.

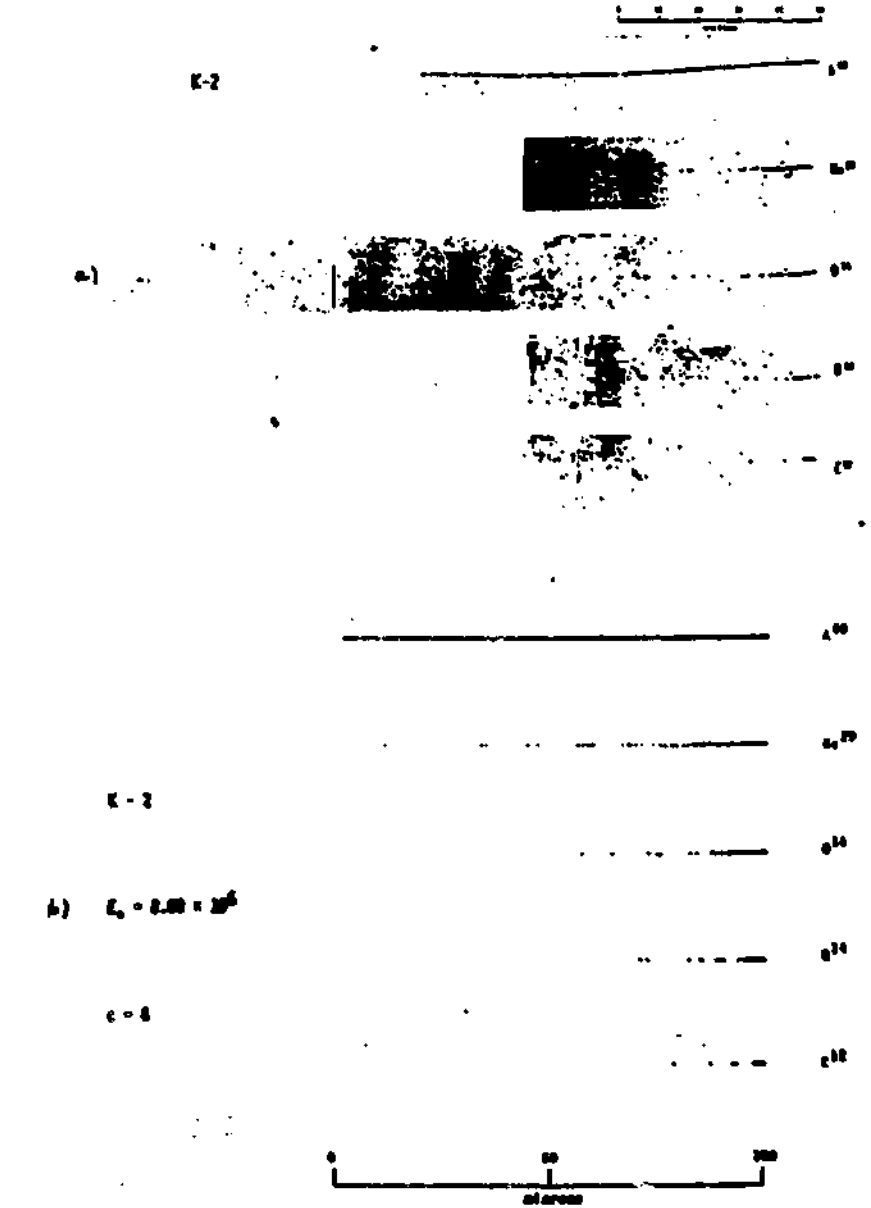

Fig 15. a) Stopping ^{40}A, ^{20}Ne, ^{16}O, ^{14}N and ^{12}C ions of initial energy 10.5 MeV/amu in Ilford K-2 emulsion; b) computer simulation of tracks of these ions, assuming this emulsion to be an 8-hit detector. From (3), courtesy R. Katz.

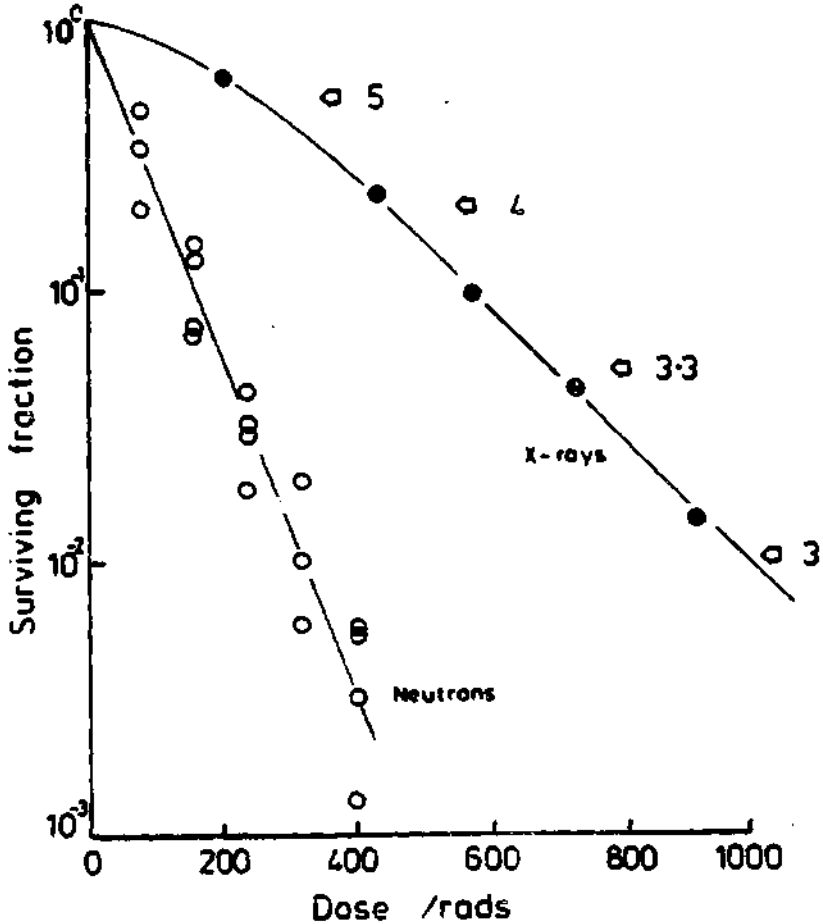

Fig. 16. Survival curves for Ehrlich ascites cells irradiated with 250 kVp X-rays or cyclotron neutrons. The lines have been drawn by eye and the numbers to the right of the X-ray survival curve represent the RBE measured at the level of the arrows. From (20).

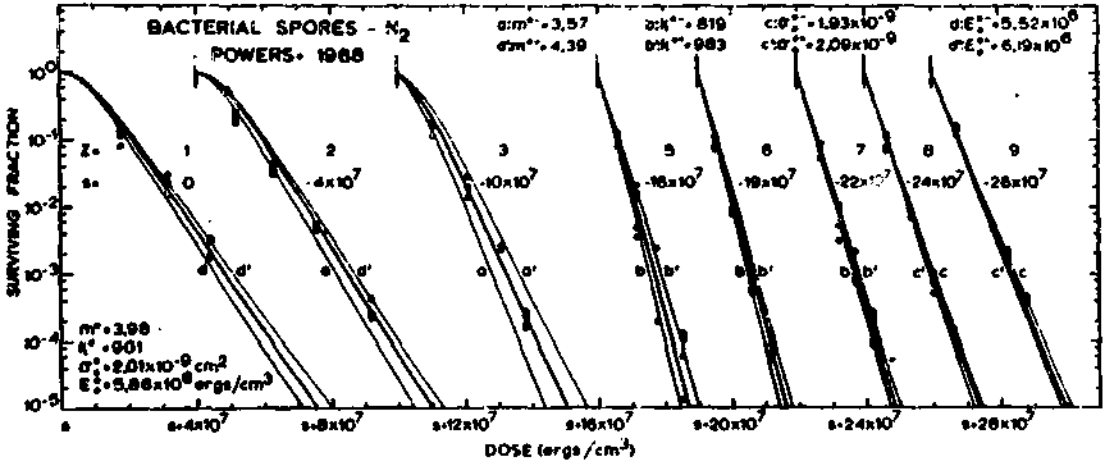

Fig. 17. Survival data for bacterial spores (anoxic) after irradiation with heavy ions, in comparison to theoretical curves generated by the four fitted radiosensitivity parameters. Also shown are the curves which would be generated by parameters bracketing 95% confidence limits (cf. table of parameters in Fig. 21). From (3), courtesy R. Katz.

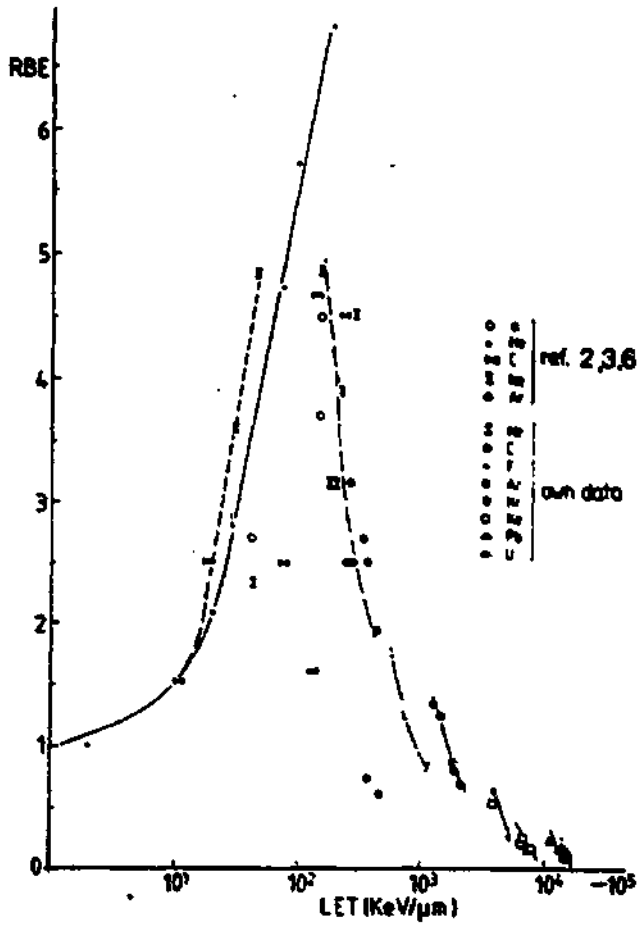

Fig. 18. Relative biological effectiveness for survival of Chinese hamster cells as a function of LET. From Wulf et al., Radiat. Res. 104, S-122-S-134 (1985).

THE MODEL

<u>radiosensitivity parameters</u>:	m, E_c, σ_c, α	
number of transformed cells:	$K = 1-N/N_0$	(1)
surviving frantion in grain-count regime:	$1-K = N/N_0 = \Pi_I \times \Pi_\gamma$	(2)
ion-kill mode survival probability:	$\Pi_I = \exp(-\sigma F)$	(3)
gamma-kill mode survival probability:	$\Pi_\gamma = 1 - (1 - \exp(-D_\gamma/E_c))^m$	(4)
gamma-kill dose fraction:	$D_\gamma = (1 - P)D$	(5)
	$P = \sigma/\sigma_0 = (1 - \exp(-Z^{*2}/\alpha\beta^2))^m$	(6)
track width regime($P > 0.98$):	$\Pi_\gamma = 1$	(7)
radiobiological effectiveness:	$RBE = D_X/D$	(8)
	$D_X = E_c(\ln(1 - (1-N/N_0)^{1/m}))$	(9)
	$D = F L$	(10)
effective charge:	$Z^* = Z(1-\exp(-125\beta Z^{-2/3}))$	(11)
stopping power(LET_∞):	$L(Z,\beta) = L_p(\beta)(Z^*/Z_p)^2$	(12)
ion range:	$R(Z,\beta) = (AMU/Z^2)(R_p(\beta)+C(\beta))$	(13)

Fig. 19. Equations of the cellular track structure theory.

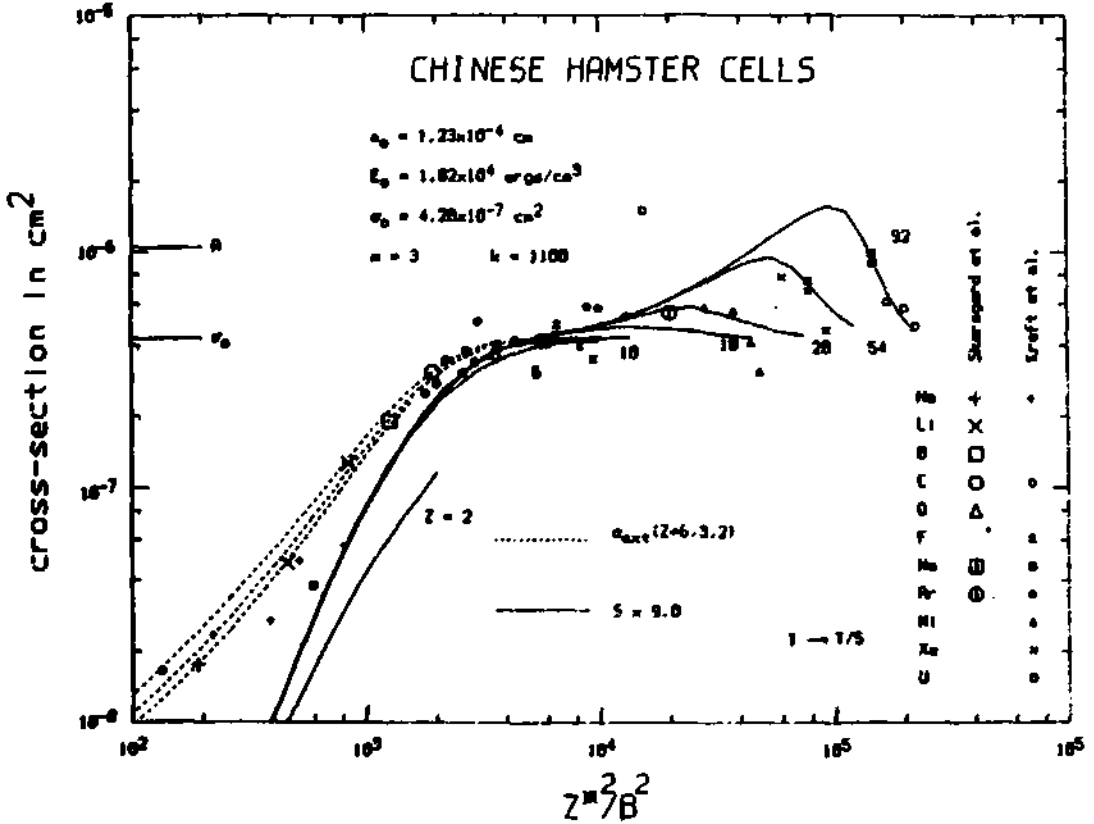

Fig. 20. Inactivation cross sections for Chinese hamster cells, an example of a theoretical fit to experimental data. Note the calculated ion-kill cross-section (full lines) first rising cubically in the grain count regime, saturating and rising further in the track width regime, and finally decreasing due to thindown. Broken lines are calculated values of the extrapolated cross section. From (41), courtesy R. Katz.

		β	E_0	±*	Δ%†	σ_0	±*	Δ%†	m	±*	Δ%†	κ	±*	Δ%†	$E_0\sigma_0/\kappa$	±*
		pic	erg/cm³			cm²									erg/cm	
BACTERIAL SPORES	N_2	110	6.06×10^{5}	± 6%	1	2.01×10^{-9}	± 4%	1	3.58	± 10%	1	901	± 9%	5	1.3×10^{-5}	± 7%
	O_2	170	4.44	± 6%	1	1.98	± 3%	1	3.82	± 12%	5	861	± 11%	8	1.1	± 5%
	N_2§	174	1.16×10^{7}	± 4%	5	1.09	± 4%	1	3.99	± 7%	4	1099	± 7%	8	2.1	± 6%
DIPLOID YEAST X841	N_2	[illegible]	[illegible]	[illegible]	[illegible]	[illegible]	[illegible]	[illegible]	[illegible]	[illegible]	[illegible]	[illegible]	[illegible]	[illegible]		
	O_2	63	2.32	± 16%	7	4.17	± 15%	19	3.07	± 21%	2	1271	± 24%	10	0.8	± 19%
DIPLOID YEAST [illegible]	N_2	27	1.38	± 59%	14	1.67×10^{-8}	± 14%	34	3.17	± 74%	4	1406	± 80%	26	1.6	± 40%
	O_2	35	1.01	± 7%	12	1.60	± 9%	32	2.23	± 3%	24	1345	± 1%	40	1.1	± 7%
HELA	O_2	72	1.34×10^{6}	± 8%	4	5.94×10^{-7}	± 9%	6	2.02	± 10%	3	755	± 20%	1	1.1	± 10%
CHANG LIVER	O_2	34	1.10	± 9%	8	4.09	± 26%	12	1.00	± 4%	20	824	± 19%	6	0.8	± 16%
HAMSTER	O_2	233	1.03	± 3%	4	4.28	± 8%	7	2.07	± 9%	19	1115	± 11%	20	0.7	± 7%
T-1 KIDNEY	N_2	[illegible]	[illegible]	[illegible]	[illegible]	[illegible]	[illegible]	[illegible]	[illegible]	[illegible]	[illegible]	[illegible]	[illegible]	[illegible]		
	O_2	62	1.41	± 14%	26	4.21×10^{-7}	± 44%	22	3.13	± 39%	25	957	± 57%	32	0.4	± 47%
T-1 KIDNEY ([illegible])	N_2	32	4.60	± 80%	0	0.72	± 30%	27	2.01	± 35%	20	1910	± 63%	40	1.9	± 32%
	O_2	81	1.16	± 7%	4	0.50	± 7%	3	2.44	± 8%	2	1083	± 17%	6	0.9	± 11%
T-1 KIDNEY - [illegible]	N_2	[illegible]	[illegible]	[illegible]	[illegible]	[illegible]	[illegible]	[illegible]	[illegible]	[illegible]	[illegible]	[illegible]	[illegible]	[illegible]		
	O_2	34	0.99×10^{3}	± 8%	0	7.01	± 16%	5	2.53	± 29%	5	865	± 45%	5	0.8	± 26%
LEUKEMIA [illegible]	N_2	[illegible]	[illegible]	[illegible]	[illegible]	[illegible]	[illegible]	[illegible]	[illegible]	[illegible]	[illegible]	[illegible]	[illegible]	[illegible]		
	O_2	[illegible]	[illegible]	[illegible]	[illegible]	[illegible]	[illegible]	[illegible]	[illegible]	[illegible]	[illegible]	[illegible]	[illegible]	[illegible]		
T. CONFUSUM EGGS	O_2	[illegible]	[illegible]	[illegible]	[illegible]	[illegible]	[illegible]	[illegible]	[illegible]	[illegible]	[illegible]	[illegible]	[illegible]	[illegible]		
HAPLOID YEAST	O_2	16	3.70×10^{8}	± 15%	8	1.31×10^{-9}	± 11%	1	2.10	± 31%	9	1804	± 30%	4	0.3	± 29%
NONBUDDING YEAST	O_2	80	1.00	± 30%	9	1.26	± 30%	26	1.76	± 45%	12	1841	± 88%	74	0.1	± 39%
E.COLI [illegible]*	O_2	40	3.03	± 7%	4	3.50×10^{-9}	± 6%	7	1.60	± 30%	8	722	± 30%	3	0.2	± 12%

* 95% Confidence Limits

† Percentage Deviation from Visually Fitted Parameters

Fig. 21. Celular radiosensitivity parameters, as fitted numerically to cell survival data. From (3), courtesy R. Katz.

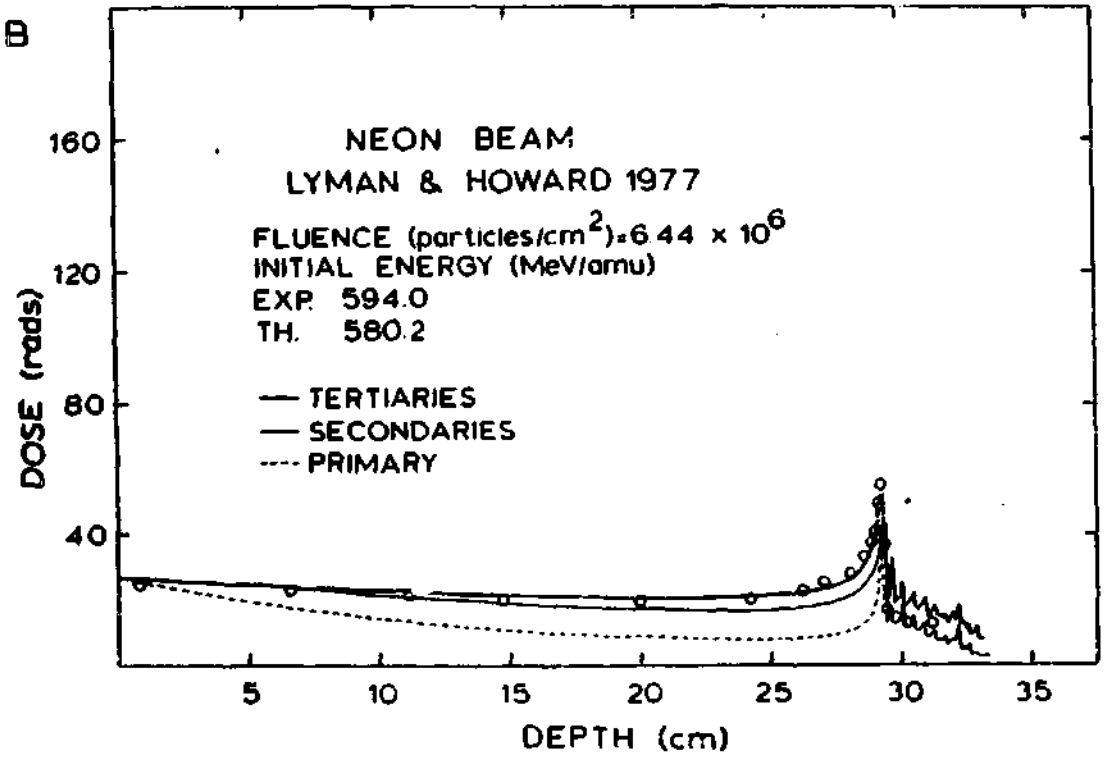

Fig. 22. Calculated dose as a function of depth, compared to experimental data (open circles) for a 594 MeV/amu Ne beam. The energy chosen for the calculation (580.2 MeV/amu) gives best agreement between calculated and measured doses. From (26), courtesy R. Katz.

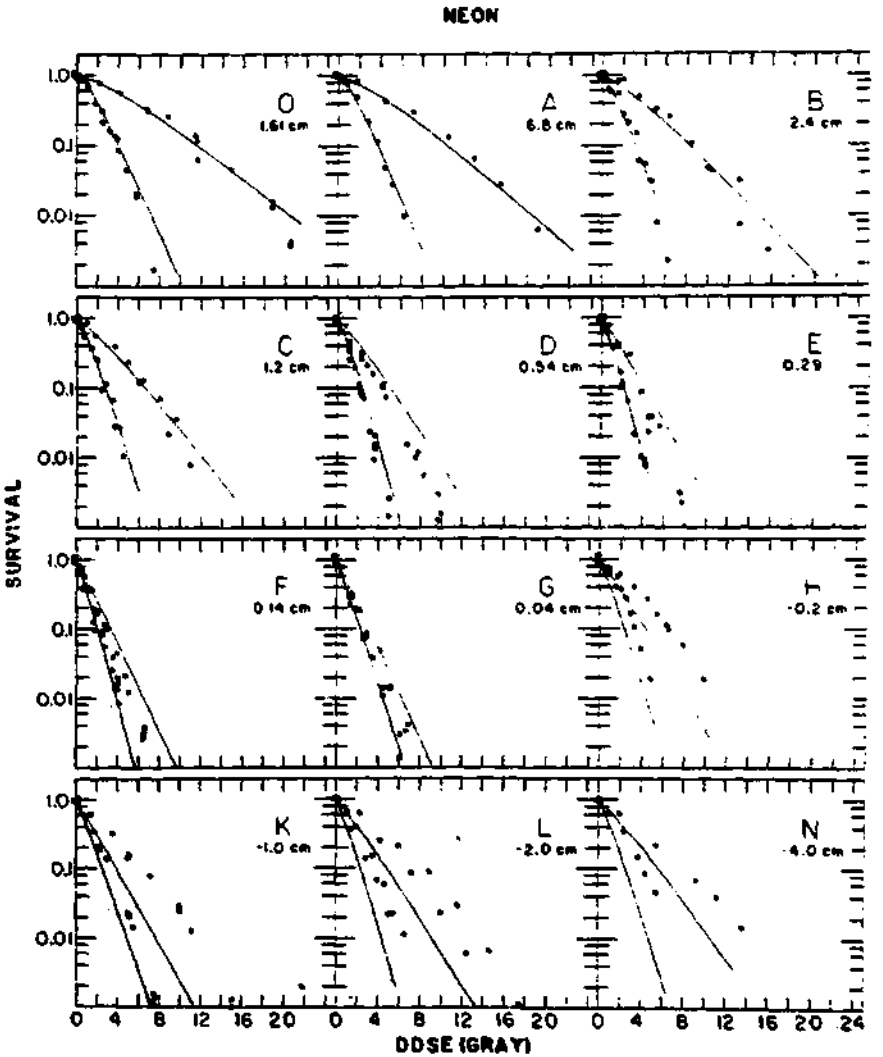

Fig. 23. Survival curves for T-1 human kidney cells in the neon beam of Fig. 22. The data, from Blakely et al., Radiat. Res. 80, 122-160 (1979), for hypoxic cells shown as open squares .those for aerobically irradiated cells shown as solid squares. Lines are calculated from theory and the beam model. From (26), courtesy R. Katz.

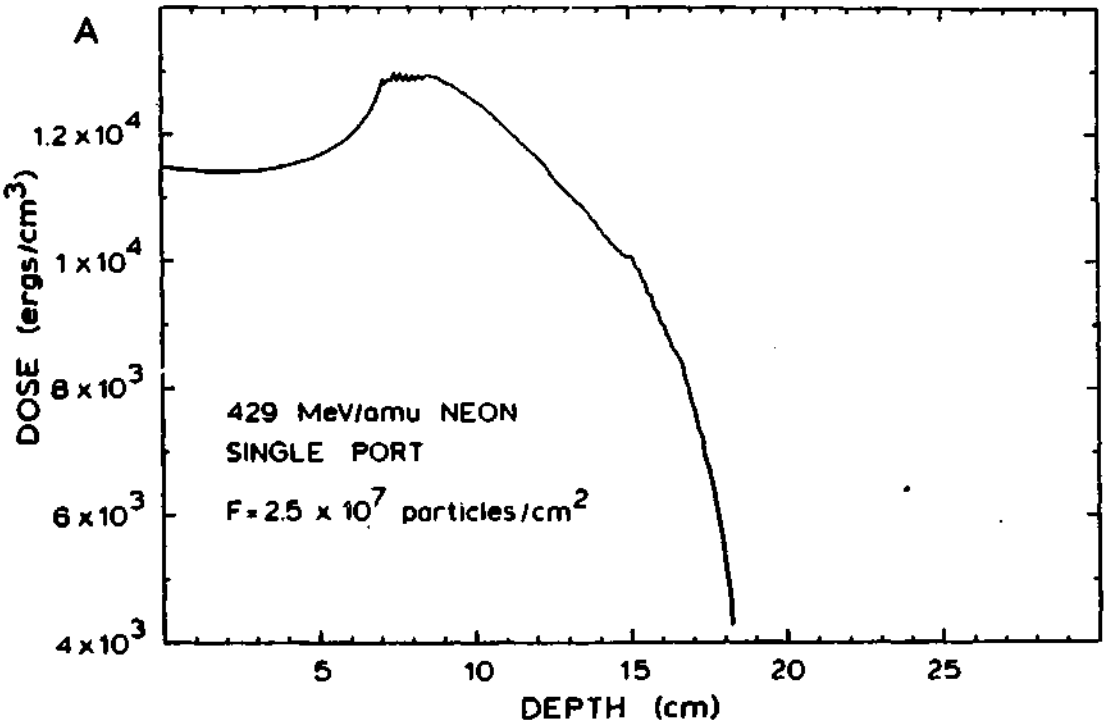

Fig. 24. Dose-depth distribution ... a single-port filtered 429 MeV/amu Ne beam calculated from the beam model (25). Courtesy R. Katz.

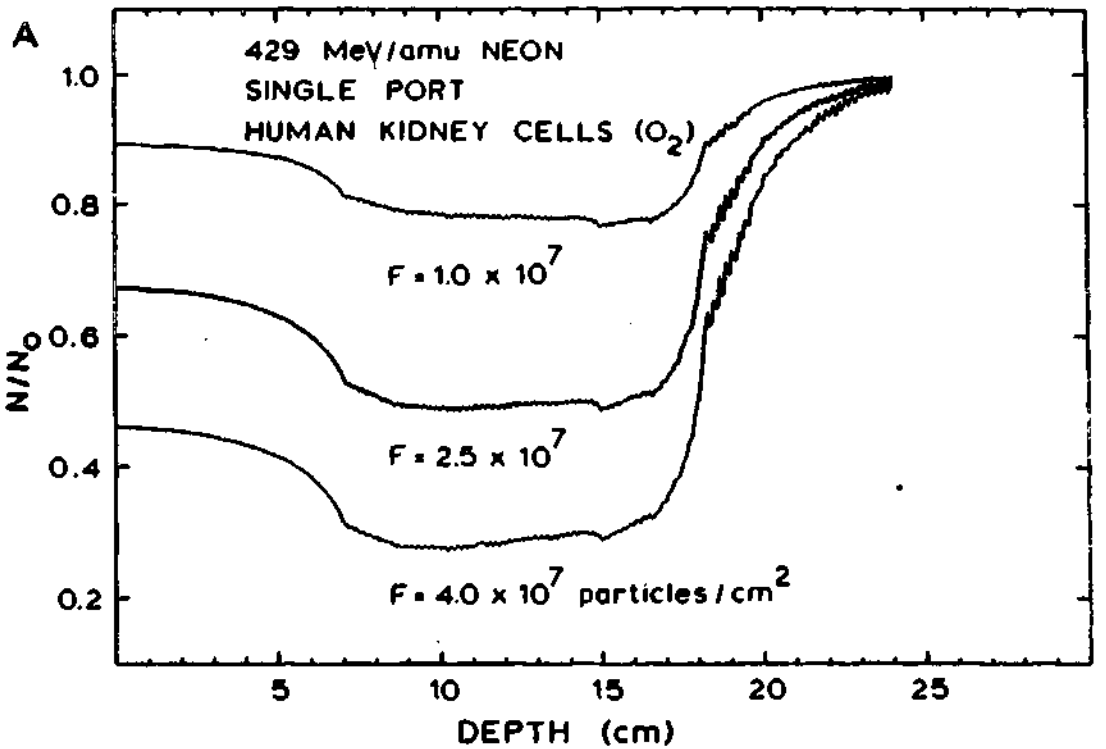

Fig. 25. Survival-depth distributions for T-1 human kidney cells, after different fluences (doses) from the beam of Fig. 24. Courtesy R. Katz.

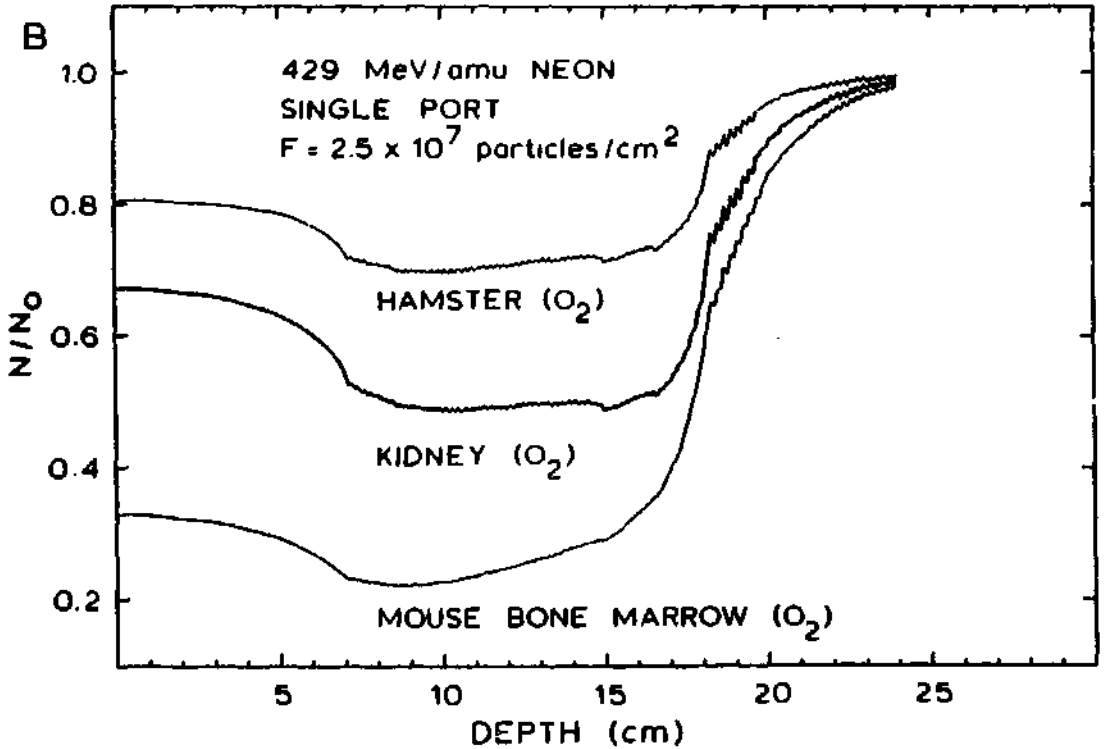

Fig. 26. Survival-depth distributions for different cell lines after a fluence 2.5 x 10^7 particles/cm² from the beam of Fig. 24. Courtesy R. Katz.

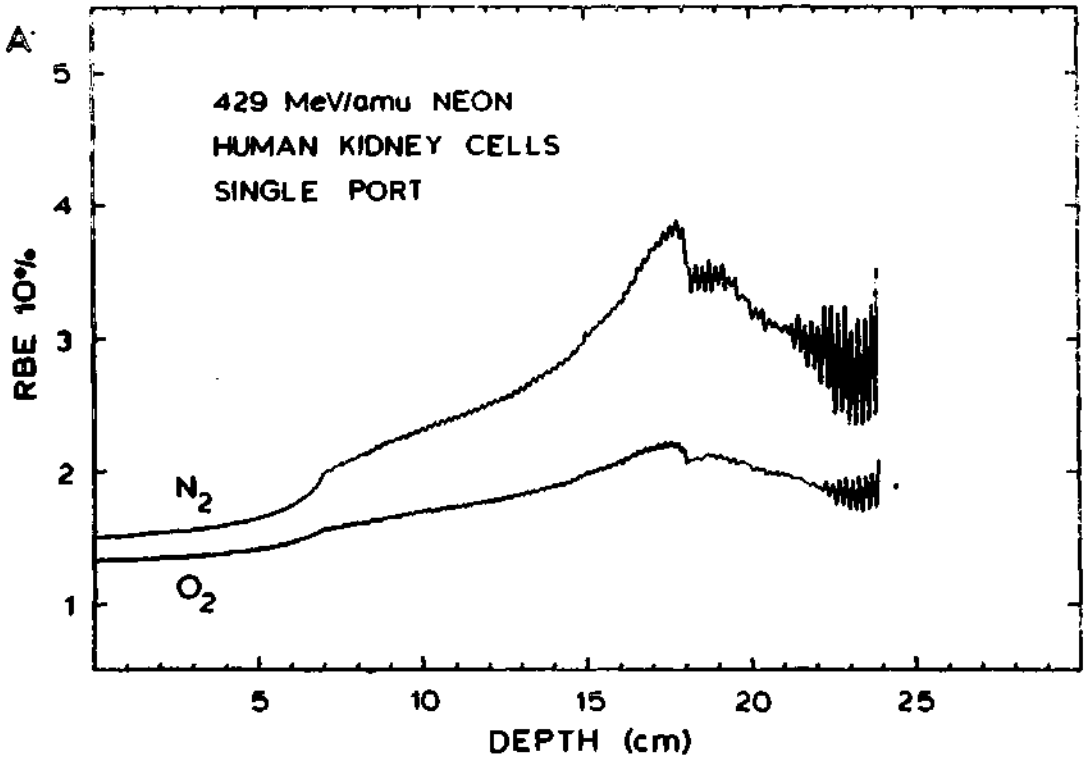

Fig. 27. Depth distribution of RBE at 10% survival for anoxic (N_2) and aerobic (O_2) T-1 human kidney cells, for the beam of Fig. 24. Courtesy R. Katz.

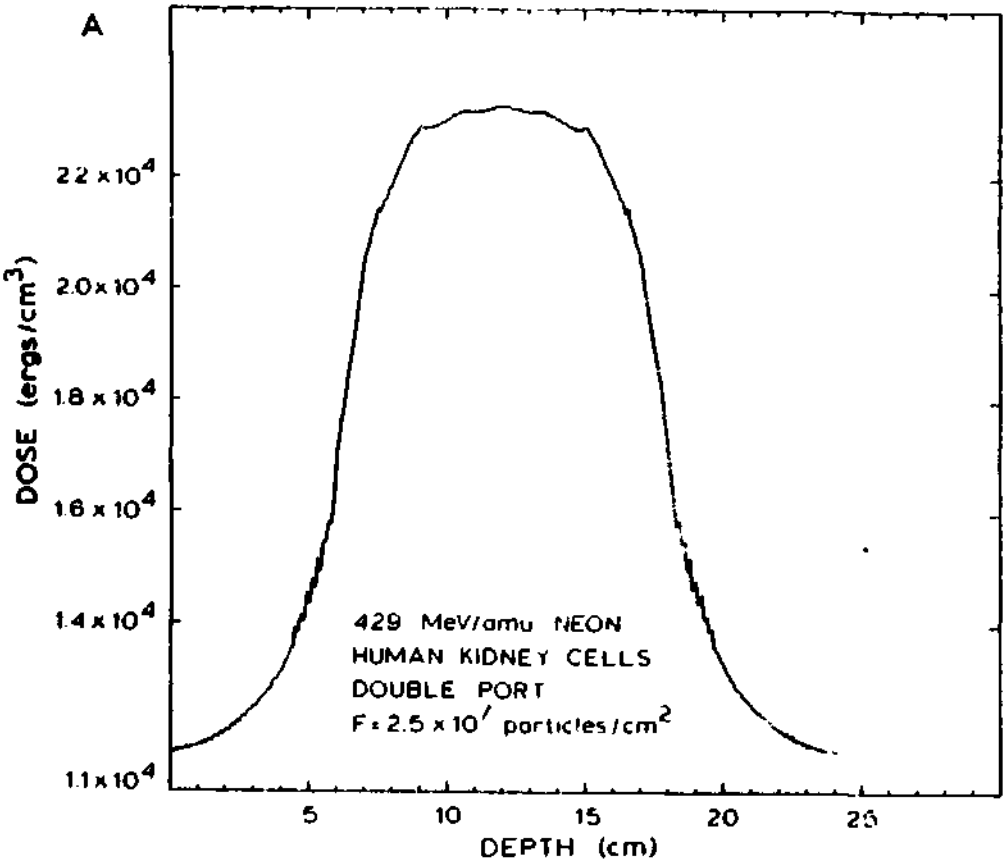

Fig. 28. Dose-depth distribution for a [illegible] port filtered 429 MeV/amu Ne beam [illegible]

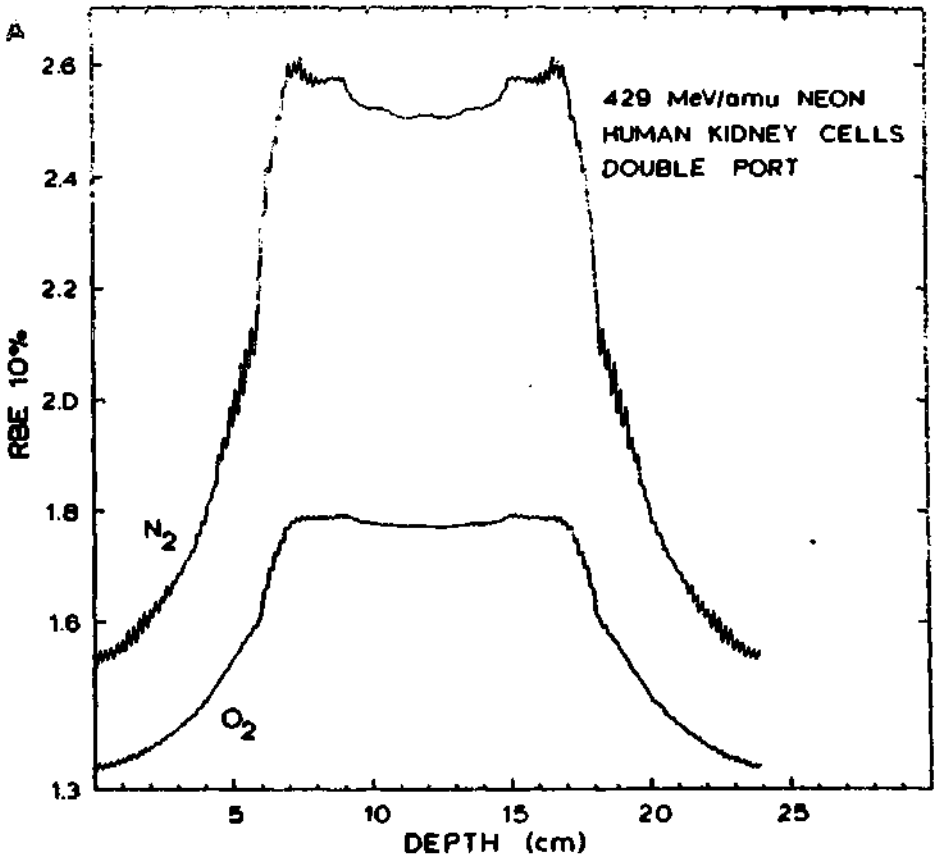

Fig. 29. Depth distribution of RBE at 10% survival for anoxic (N_2) and aerobic (O_2) T-1 human kidney cells, for the beam of Fig. 28. Courtesy R. Katz.

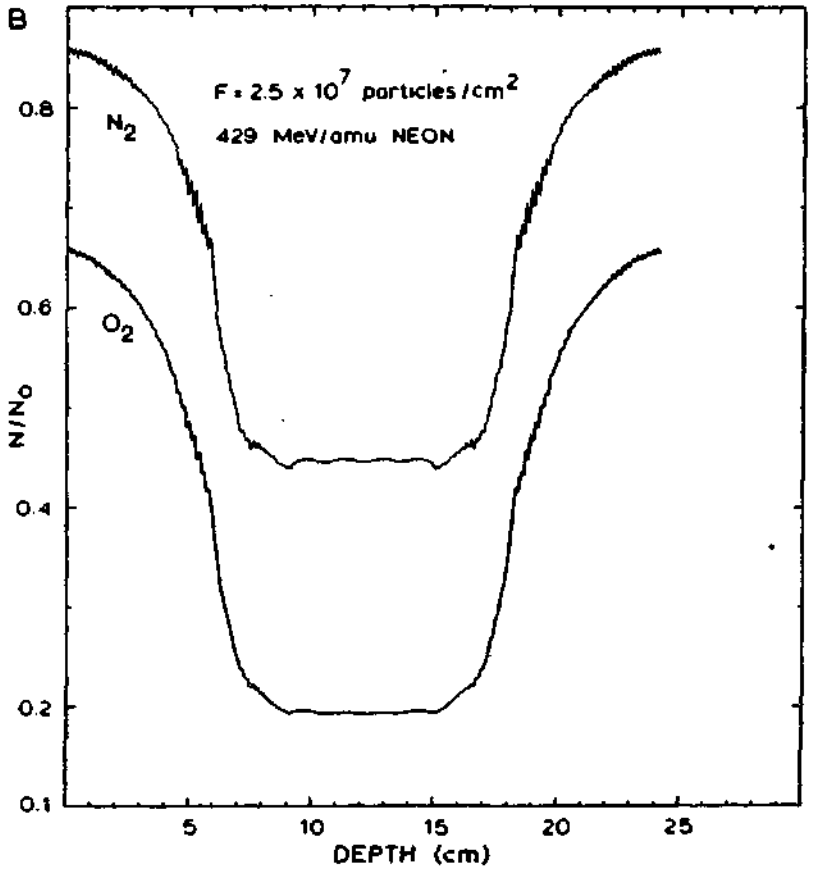

Fig. 30. Depth distribution of survival for anoxic (N_2) and aerobic (O_2) T-1 human kidney cells, for the beam of Fig. 28, at beam fluence 2.5 x 10^7 particles/cm^2. Courtesy R. Katz.

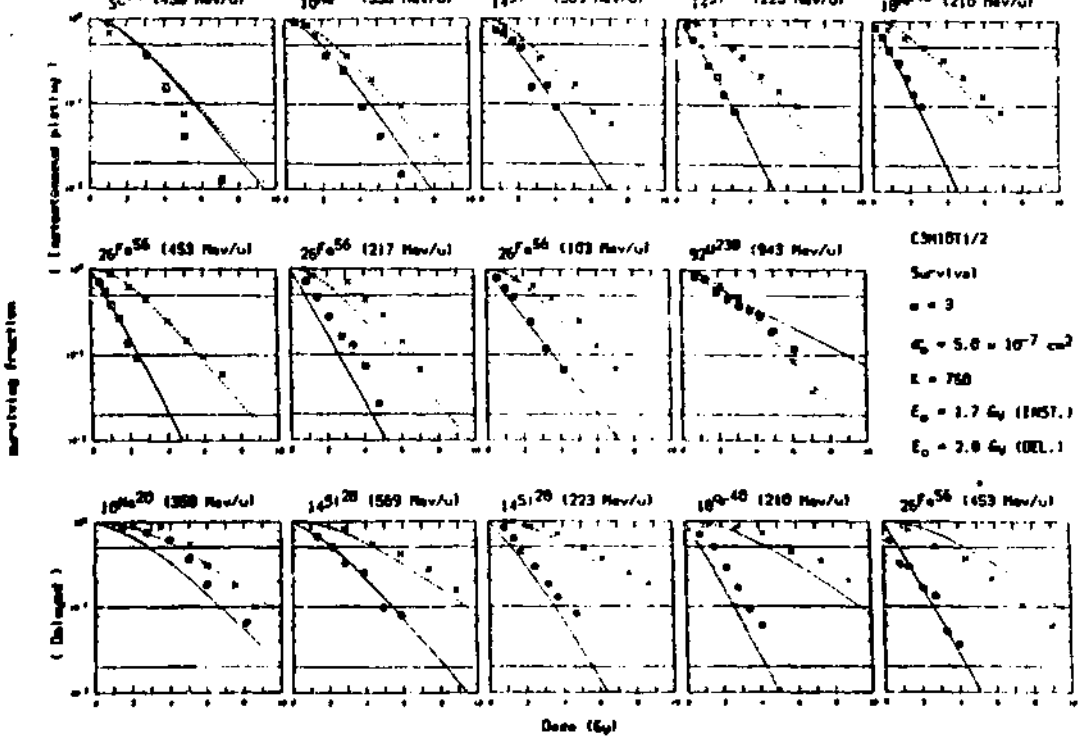

Fig. 31. Measured (2B) and calculated survival fraction of C3H10T1/2 cells after irradiation with X rays (X) and BEVALAC ions, for instantaneous (squares) and delayed (circles) plating. Above each box the ion and beam energy are given. Full lines represent model calculations using parameters listed in the figure. From (9).

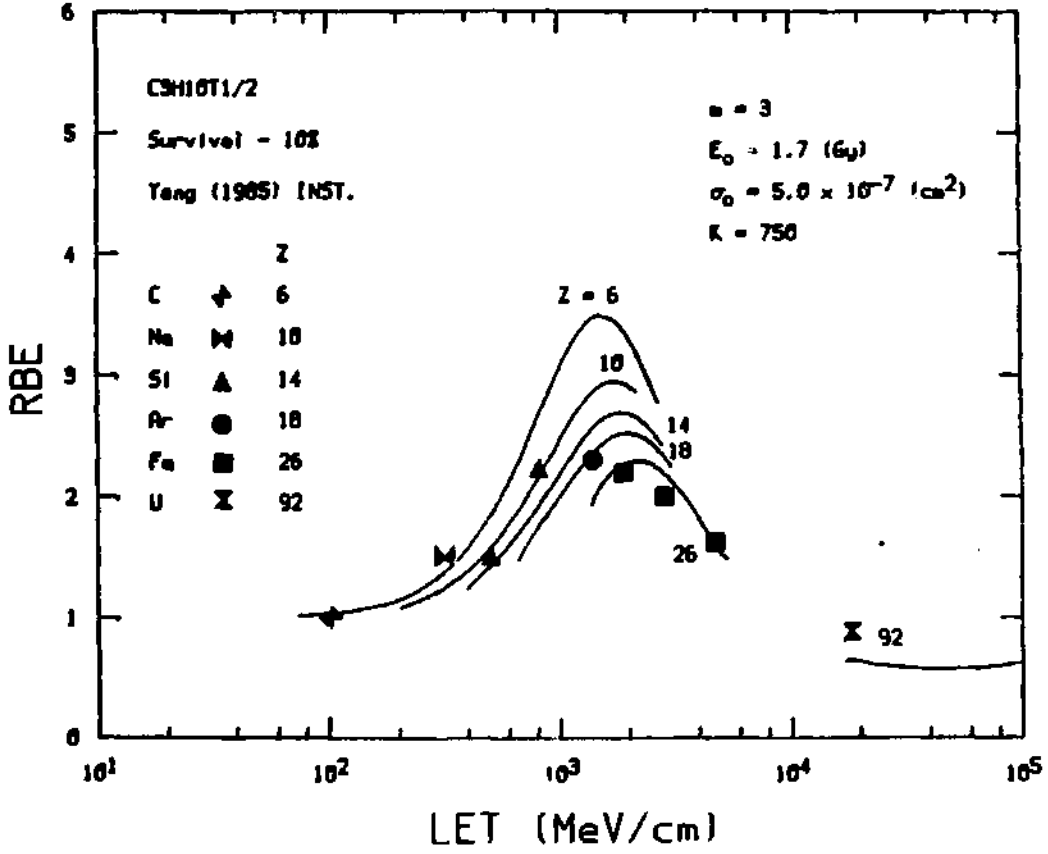

Fig. 32. Measured (2D) and calculated (4P) of 10% survival for C3H10T1/2 cells plated immediately after irradiation. From (9).

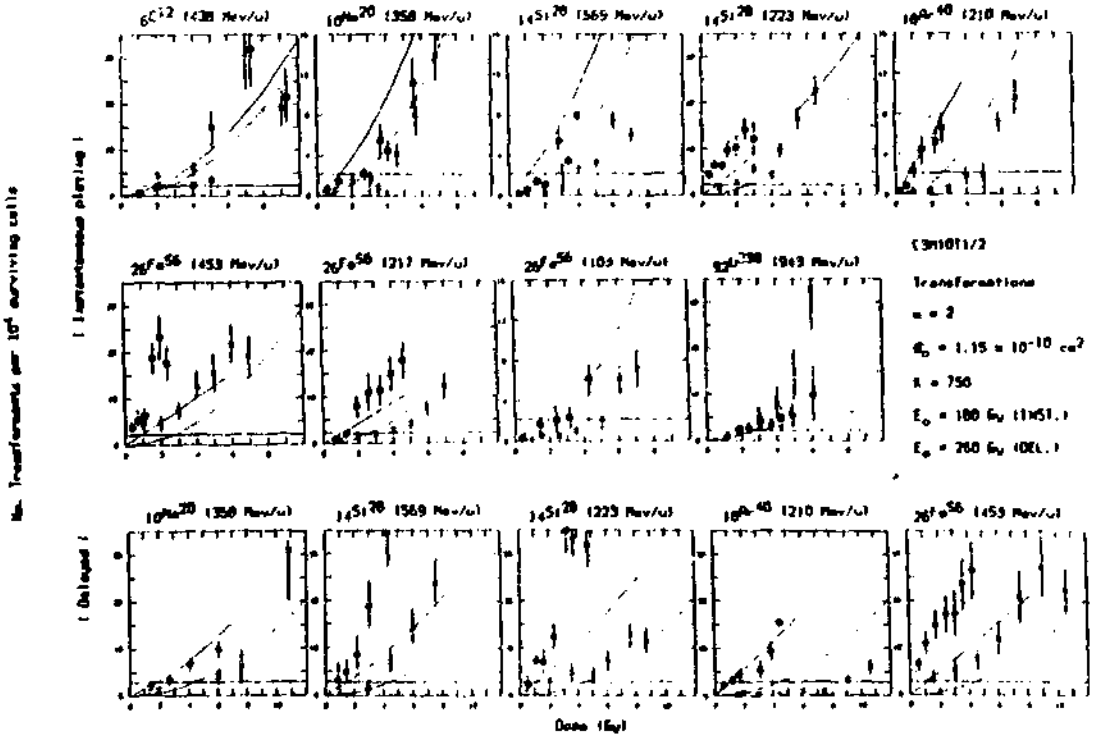

Fig. 33. Measured (2σ) and calculated transformation frequencies in C3H10T1/2 cells after irradiation with X-rays (X) and BEVALAC ions, for instantaneous (squares) and delayed (circles) plating. Above each box the ion and beam energy are given. Full lines represent model calculations using parameters listed in the figure. From (9).

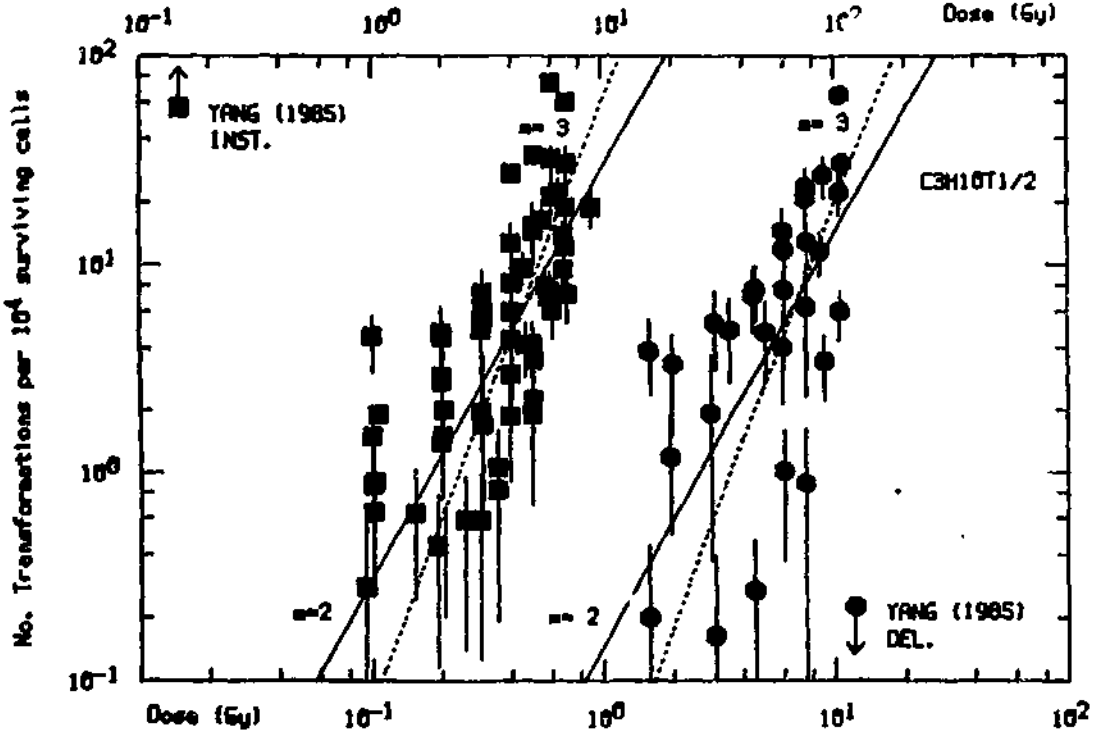

Fig. 34. Measured (2B) transformation frequencies in C3H10T1/2 cells after X-ray doses, for instantaneous (INST-upper abscissa) and delayed (DEL-lower abscissa) plating. Data are pooled from all experiments. Full line represents the m=2-target model ($E_{0,inst}$=180 Gy, $E_{0,del}$=260 Gy), broken line represents the the m=3-target model ($E_{0,inst}$=50 Gy, $E_{0,del}$=75 Gy). From (9).

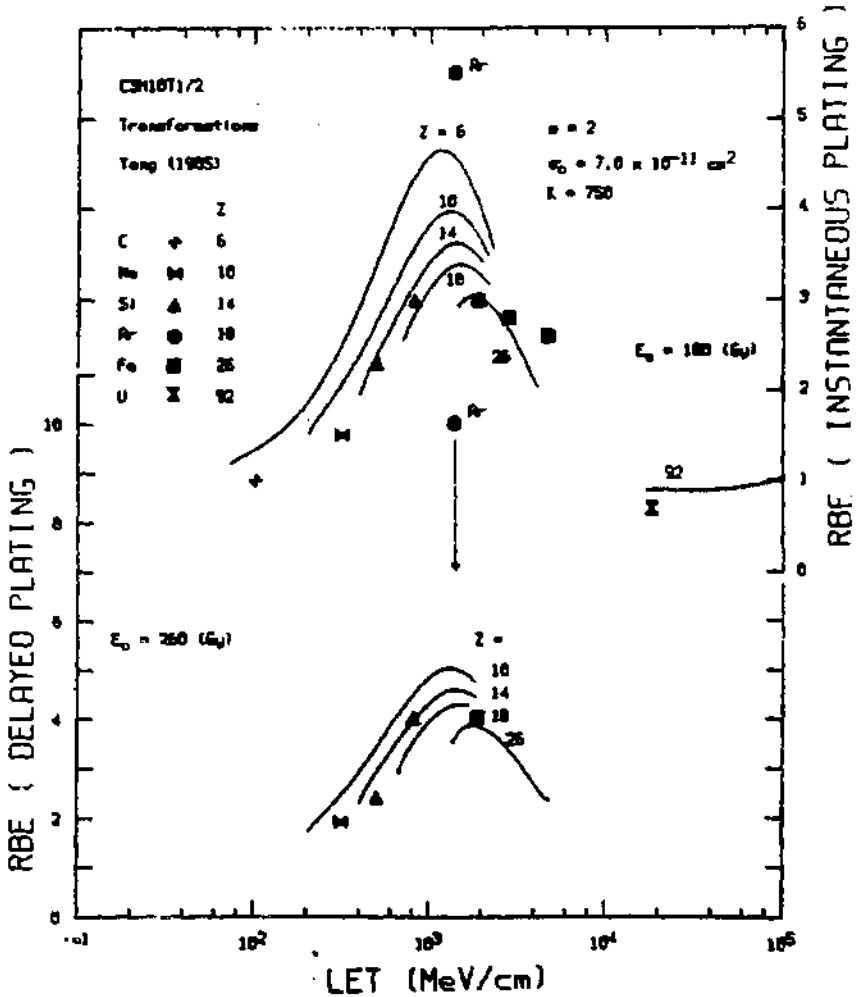

Fig. 35. Measured (28) and calculated RBE for transformations in C3H10T1/2 cells at levels corresponding to 50% survival, for instantaneous (upper panel, upper right-hand ordinate) and delayed (lower panel, lower left-hand ordinate) plating. From (9).

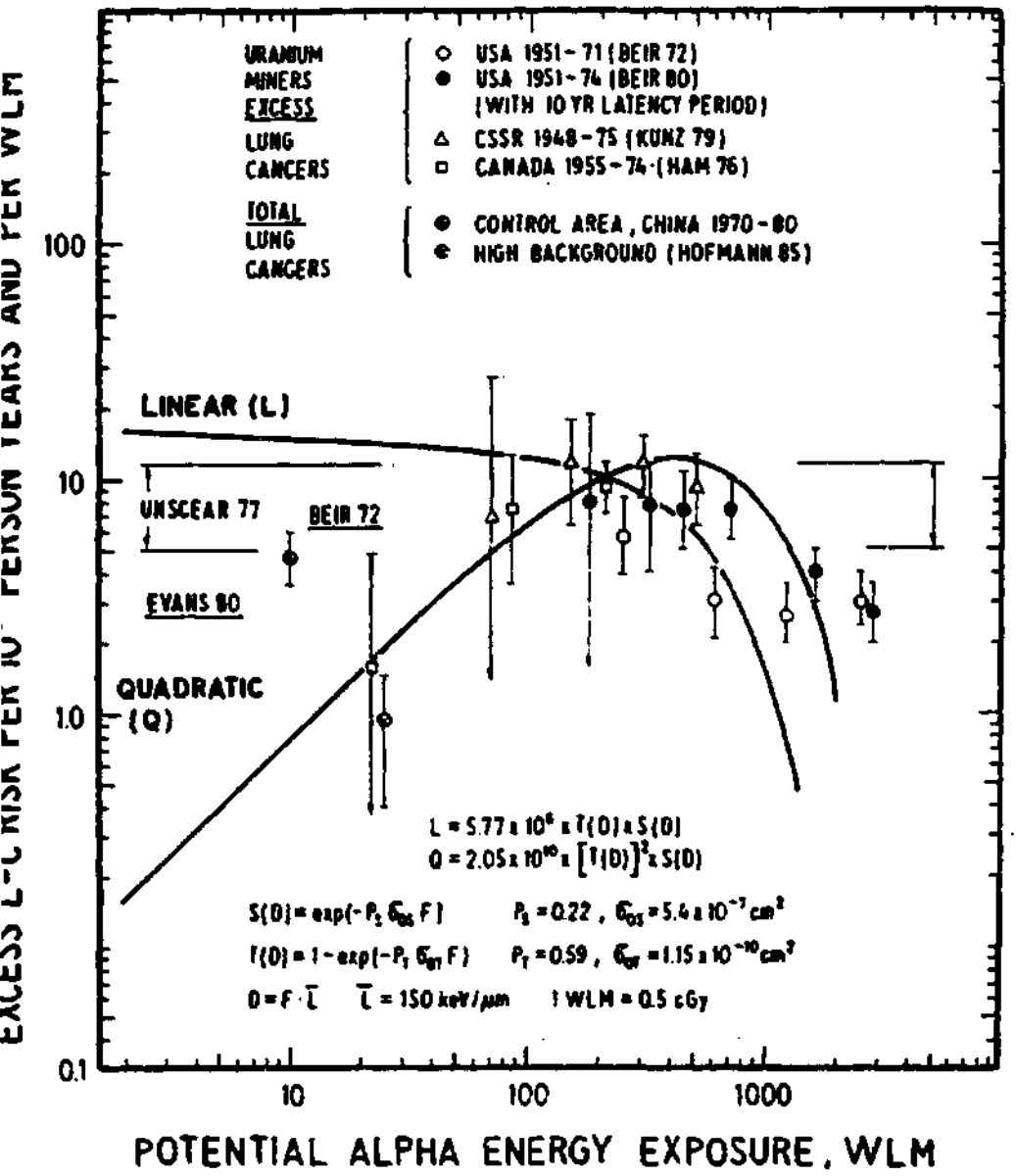

ig. 36. Excess lung cancer risk in uranium miners and total lung cancer risk in the inhabitants in high background areas in China vs. cumulative exposure to radon and thoron decay products in WLM. Theoretical curves are normalized to the same value at 200 WLM. Data points are taken from Hofmann, Katz and Zhang (29). From (1).

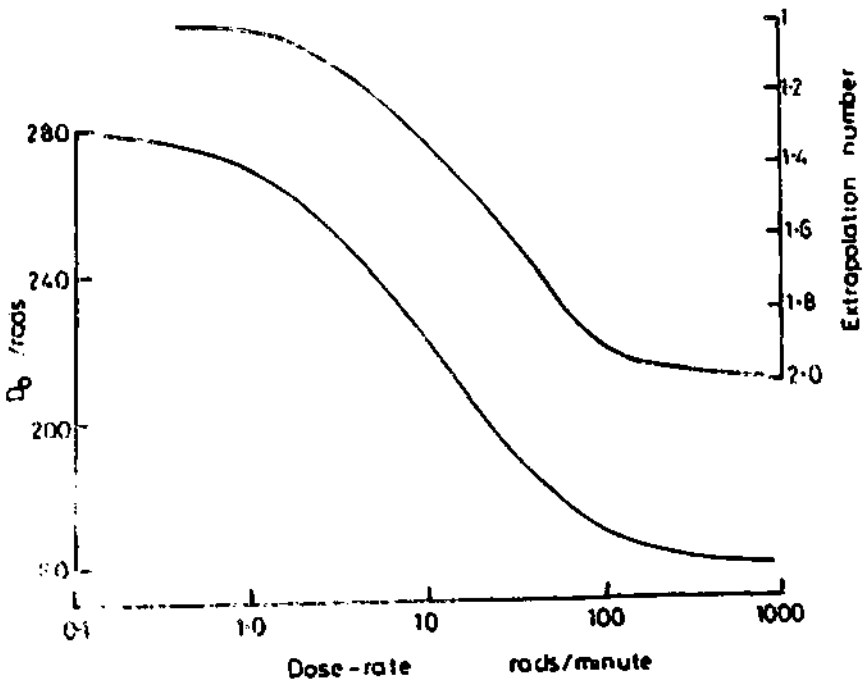

Fig. 37. Dependence of E_0 and extrapolation number m on the dose-rate for HeLa cells exposed to gamma rays in air. From (20).

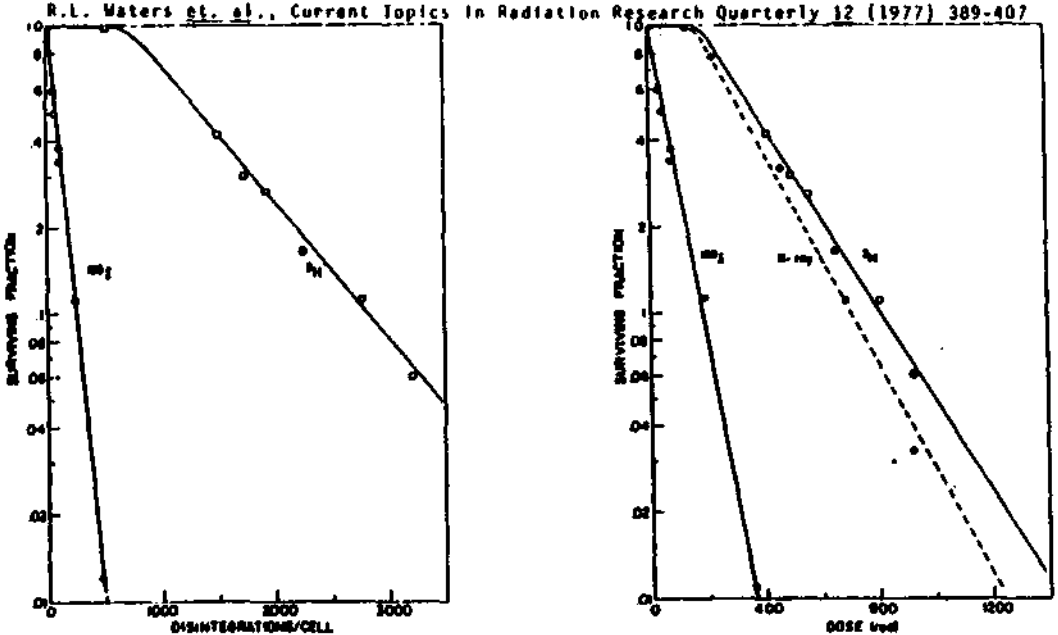

Fig. 38. Fraction of CHO cells surviving various doses of ^{3}H-IdR, ^{125}I-UdR or external X-rays, plotted as a function of cumulative disintegrations per cell (left) or as a function of radiation dose (rad) to the cell nucleus (right). From R. L. Waters et al. Current Topics in Rad. Res. Quart. 12, 389-407 (1977).

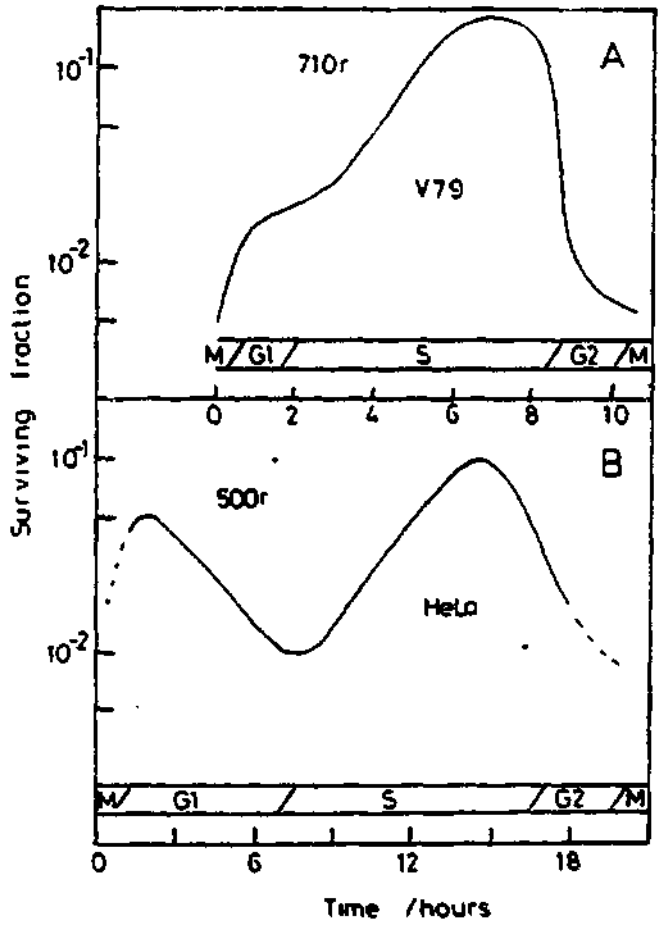

Fig. 39. The age-response function for V79 cells and HeLa cells exposed to single doses of radiation. From W. K. Sinclair, Radiat. Res. 33, 620 (1968), after (20).